

ENGINEERING OF BIOMATERIALS

INŻYNIERIA BIOMATERIAŁÓW

JOURNAL OF POLISH SOCIETY FOR BIOMATERIALS AND FACULTY OF MATERIALS SCIENCE AND CERAMICS AGH-UST

CZASOPISMO POLSKIEGO STOWARZYSZENIA BIOMATERIAŁÓW I WYDZIAŁU INŻYNIERII MATERIAŁOWEJ I CERAMIKI AGH

Number 161

Numer 161

Volume XXIV

Rok XXIV

JULY 2021

LIPIEC 2021

ISSN 1429-7248

PUBLISHER:

WYDAWCA:

**Polish Society
for Biomaterials
in Krakow**

Polskie
Stowarzyszenie
Biomateriałów
w Krakowie

**EDITORIAL
COMMITTEE:**

KOMITET
REDAKCYJNY:

Editor-in-Chief

Redaktor naczelny
Elżbieta Pamuła

Editor

Redaktor
**Patrycja
Domalik-Pyzik**

Secretary of editorial

Sekretarz redakcji

Design

Projekt
Katarzyna Trała

**ADDRESS OF
EDITORIAL OFFICE:**

ADRES REDAKCJI:

AGH-UST

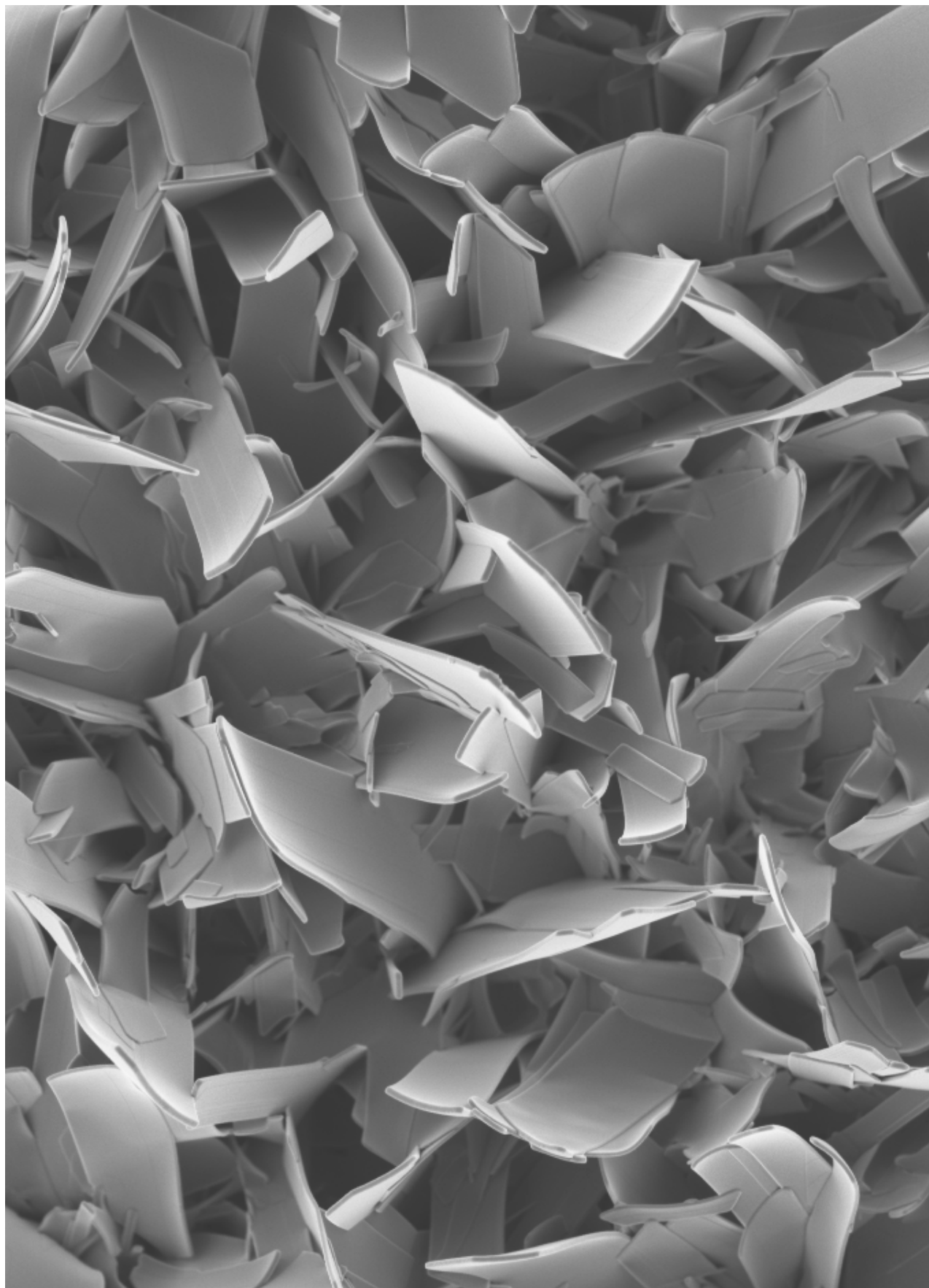
30/A3, Mickiewicz Av.
30-059 Krakow, Poland
Akademia
Górnictwo-Hutnicza
al. Mickiewicza 30/A-3
30-059 Kraków

Issue: 250 copies

Nakład: 250 egz.

**Scientific Publishing
House AKAPIT**

Wydawnictwo Naukowe
AKAPIT
e-mail: wn@akapit.krakow.pl



**EDITORIAL BOARD
KOMITET REDAKCYJNY**

EDITOR-IN-CHIEF

Elżbieta Pamuła - AGH UNIVERSITY OF SCIENCE AND TECHNOLOGY, KRAKOW, POLAND

EDITOR

Patrycja Domalik-Pyzik - AGH UNIVERSITY OF SCIENCE AND TECHNOLOGY, KRAKOW, POLAND

**INTERNATIONAL EDITORIAL BOARD
MIĘDZYNARODOWY KOMITET REDAKCYJNY**

Iulian Antoniac - UNIVERSITY POLITEHNICA OF BUCHAREST, ROMANIA

Lucie Bacakova - ACADEMY OF SCIENCE OF THE CZECH REPUBLIC, PRAGUE, CZECH REPUBLIC

Romuald Będziński - UNIVERSITY OF ZIELONA GÓRA, POLAND

Marta Błażewicz - AGH UNIVERSITY OF SCIENCE AND TECHNOLOGY, KRAKOW, POLAND

Stanisław Błażewicz - AGH UNIVERSITY OF SCIENCE AND TECHNOLOGY, KRAKOW, POLAND

Wojciech Chrzanowski - UNIVERSITY OF SYDNEY, AUSTRALIA

Jan Ryszard Dąbrowski - BIAŁYSTOK TECHNICAL UNIVERSITY, POLAND

Timothy Douglas - LANCASTER UNIVERSITY, UNITED KINGDOM

Christine Dupont-Gillain - UNIVERSITÉ CATHOLIQUE DE LOUVAIN, BELGIUM

Matthias Epple - UNIVERSITY OF DUISBURG-ESSEN, GERMANY

Robert Hurt - BROWN UNIVERSITY, PROVIDENCE, USA

James Kirkpatrick - JOHANNES GUTENBERG UNIVERSITY, MAINZ, GERMANY

Ireneusz Kotela - CENTRAL CLINICAL HOSPITAL OF THE MINISTRY OF THE INTERIOR AND ADMINISTR. IN WARSAW, POLAND

Małgorzata Lewandowska-Szumieł - MEDICAL UNIVERSITY OF WARSAW, POLAND

Jan Marciniak - SILESIA UNIVERSITY OF TECHNOLOGY, ZABRZE, POLAND

Ion N. Mihailescu - NATIONAL INSTITUTE FOR LASER, PLASMA AND RADIATION PHYSICS, BUCHAREST, ROMANIA

Sergey Mikhalovsky - UNIVERSITY OF BRIGHTON, UNITED KINGDOM

Stanisław Mitura - TECHNICAL UNIVERSITY OF LIBEREC, CZECH REPUBLIC

Piotr Niedzielski - TECHNICAL UNIVERSITY OF LODZ, POLAND

Abhay Pandit - NATIONAL UNIVERSITY OF IRELAND, GALWAY, IRELAND

Stanisław Pielka - WROCLAW MEDICAL UNIVERSITY, POLAND

Vehid Salih - UCL EASTMAN DENTAL INSTITUTE, LONDON, UNITED KINGDOM

Jacek Składzień - JAGIELLONIAN UNIVERSITY, COLLEGIUM MEDICUM, KRAKOW, POLAND

Andrei V. Stanishevsky - UNIVERSITY OF ALABAMA AT BIRMINGHAM, USA

Anna Ślósarczyk - AGH UNIVERSITY OF SCIENCE AND TECHNOLOGY, KRAKOW, POLAND

Tadeusz Trzaska - UNIVERSITY SCHOOL OF PHYSICAL EDUCATION, POZNAŃ, POLAND

Dimitris Tsipas - ARISTOTLE UNIVERSITY OF THESSALONIKI, GREECE

Wskazówki dla autorów

1. Prace do opublikowania w kwartalniku „Engineering of Biomaterials / Inżynieria Biomateriałów” przyjmowane będą wyłącznie w języku angielskim.

2. Wszystkie nadsyłane artykuły są recenzowane.

3. Materiały do druku prosimy przysyłać za pomocą systemu online (www.biomaterials.pl).

4. Struktura artykułu:

• TYTUŁ • Autorzy i instytucje • Streszczenie (200-250 słów) • Słowa kluczowe (4-6) • Wprowadzenie • Materiały i metody • Wyniki i dyskusja • Wnioski • Podziękowania • Piśmiennictwo

5. Autorzy przesyłają pełną wersję artykułu, łącznie z ilustracjami, tabelami, podpisami i literaturą w jednym pliku. Artykuł w tej formie przesyłany jest do recenzentów. Dodatkowo autorzy proszeni są o przesłanie materiałów ilustracyjnych (rysunki, schematy, fotografie, wykresy) w oddzielnych plikach (format np. .jpg, .gif, .tiff, .bmp). Rozdzielczość rysunków min. 300 dpi. Wszystkie rysunki i wykresy powinny być czarno-białe lub w odcieniach szarości i ponumerowane cyframi arabskimi. W tekście należy umieścić odnośniki do rysunków i tabel.

6. Na końcu artykułu należy podać wykaz piśmiennictwa w kolejności cytowania w tekście i kolejno ponumerowany.

7. Redakcja zastrzega sobie prawo wprowadzenia do opracowań autorskich zmian terminologicznych, poprawek redakcyjnych, stylistycznych, w celu dostosowania artykułu do norm przyjętych w naszym czasopiśmie. Zmiany i uzupełnienia merytoryczne będą dokonywane w uzgodnieniu z autorem.

8. Opinia lub uwagi recenzentów będą przekazywane Autorowi do ustosunkowania się. Nie dostarczenie poprawionego artykułu w terminie oznacza rezygnację Autora z publikacji pracy w naszym czasopiśmie.

9. Za publikację artykułów redakcja nie płaci honorarium autorskiego.

10. Adres redakcji:

Czasopismo

„Engineering of Biomaterials / Inżynieria Biomateriałów”

Akademia Górniczo-Hutnicza im. St. Staszica

Wydział Inżynierii Materiałowej i Ceramiki

al. Mickiewicza 30/A-3, 30-059 Kraków

tel. (48) 12 617 44 48, 12 617 25 61

tel./fax: (48) 12 617 45 41

e-mail: epamula@agh.edu.pl, kabe@agh.edu.pl

Szczegółowe informacje dotyczące przygotowania manuskryptu oraz procedury recenzowania dostępne są na stronie internetowej czasopisma:

www.biomaterials.pl

Warunki prenumeraty

Zamówienie na prenumeratę prosimy przysyłać na adres:

mgr inż. Augustyn Powroźnik

apowroz@agh.edu.pl, tel/fax: (48) 12 617 45 41

Cena pojedynczego numeru wynosi 20 PLN

Konto: Polskie Stowarzyszenie Biomateriałów

30-059 Kraków, al. Mickiewicza 30/A-3

ING Bank Śląski S.A. O/Kraków

nr rachunku 63 1050 1445 1000 0012 0085 6001

Prenumerata obejmuje 4 numery regularne i nie obejmuje numeru specjalnego (materiały konferencyjne).

Instructions for authors

1. Papers for publication in quarterly journal „Engineering of Biomaterials / Inżynieria Biomateriałów” should be written in English.

2. All articles are reviewed.

3. Manuscripts should be submitted to editorial office through online submission system (www.biomaterials.pl).

4. A manuscript should be organized in the following order:

• TITLE • Authors and affiliations • Abstract (200-250 words) • Keywords (4-6) • Introduction • Materials and Methods • Results and Discussions • Conclusions • Acknowledgements • References

5. All illustrations, figures, tables, graphs etc. preferably in black and white or grey scale should be additionally sent as separate electronic files (format .jpg, .gif, .tiff, .bmp). High-resolution figures are required for publication, at least 300 dpi. All figures must be numbered in the order in which they appear in the paper and captioned below. They should be referenced in the text. The captions of all figures should be submitted on a separate sheet.

6. References should be listed at the end of the article. Number the references consecutively in the order in which they are first mentioned in the text.

7. The Editors reserve the right to improve manuscripts on grammar and style and to modify the manuscripts to fit in with the style of the journal. If extensive alterations are required, the manuscript will be returned to the authors for revision.

8. Opinion or notes of reviewers will be transferred to the author. If the corrected article will not be supplied on time, it means that the author has resigned from publication of work in our journal.

9. Editorial does not pay author honorarium for publication of article.

10. Address of editorial office:

Journal

„Engineering of Biomaterials / Inżynieria Biomateriałów”

AGH University of Science and Technology

Faculty of Materials Science and Ceramics

30/A-3, Mickiewicz Av., 30-059 Krakow, Poland

tel. (48) 12) 617 44 48, 12 617 25 61

tel./fax: (48) 12 617 45 41

e-mail: epamula@agh.edu.pl, kabe@agh.edu.pl

Detailed information concerning manuscript preparation and review process are available at the journal's website:

www.biomaterials.pl

Subscription terms

Contact:

MSc Augustyn Powroźnik,

e-mail: apowroz@agh.edu.pl

Subscription rates:

Cost of one number: 20 PLN

Payment should be made to:

Polish Society for Biomaterials

30/A3, Mickiewicz Av.

30-059 Krakow, Poland

ING Bank Slaski S.A.

account no. 63 1050 1445 1000 0012 0085 6001

Subscription includes 4 issues and does not include special issue (conference materials).



30th Biomaterials in Medicine and Veterinary Medicine Anniversary Conference

14 – 17 October 2021 Rytro, Poland

SAVE THE DATE

14-17

OCTOBER
2021

www.biomat.agh.edu.pl



REGISTER
AND
SUBMIT
AN ABSTRACT



SPIS TREŚCI CONTENTS

CHARACTERISTICS OF PHYSICOCHEMICAL AND RHEOLOGICAL PROPERTIES OF CHITOSAN HYDROGELS BASED ON SELECTED HYDROXY ACIDS OLGA ZAVYALOVA, SANDRA GAJEWSKA, DOMINIKA DĄBROWSKA-WISŁOCKA, ALINA SIONKOWSKA	2
NEW DESIGN OF PATIENT-SPECIFIC, ANTIMICROBIAL BIOACTIVE FINGER IMPLANTS FOR DURABLE FUNCTIONAL RECONSTRUCTION AFTER AMPUTATION MARCIN DYNER, ADAM BYRSKI, ROMAN MAJOR, MACIEJ GAWLIKOWSKI, KATARZYNA KASPERKIEWICZ, JUERGEN M. LACKNER, ANETA DYNER, BOGUSŁAW MAJOR	8
ASSESSMENT OF THE PROPERTIES OF HAp MICROPOWDERS AFTER ION EXCHANGE PROCESS IN SILVER NITRATE SOLUTION MARTA GŁUSZEK, ZUZANNA ŚWIRSKA, WITOLD KACZOROWSKI, BARTŁOMIEJ JANUSZEWICZ, MACIEJ WROTNIAK	15
THE ENCAPSULATION OF ANTIBACTERIAL DRUGS IN POLYMER NANOPARTICLES AND THEIR USE IN DRUG DELIVERY SYSTEMS ON ZrO₂ SCAFFOLD WITH BIOACTIVE COATING IWONA PUDEŁKO, GAËLLE DESANTE, ELŻBIETA PAMUŁA, KAROLINA SCHICKLE, MAŁGORZATA KROK-BORKOWICZ	21

CHARACTERISTICS OF PHYSICOCHEMICAL AND RHEOLOGICAL PROPERTIES OF CHITOSAN HYDROGELS BASED ON SELECTED HYDROXY ACIDS

OLGA ZAVYALOVA^{1*} , SANDRA GAJEWSKA¹ ,
DOMINIKA DĄBROWSKA-WISŁOCKA¹ ,
ALINA SIONKOWSKA² 

¹ FACULTY OF PHARMACY, COLLEGIUM MEDICUM, NICOLAUS COPERNICUS UNIVERSITY, JURASZ 2, 85-089 BYDGOSZCZ, POLAND

² FACULTY OF CHEMISTRY, NICOLAUS COPERNICUS UNIVERSITY, GAGARIN 7, 87-100 TORUŃ, POLAND

*E-MAIL: ZAVOLG@CM.UMK.PL

Abstract

Chitosan is a natural cationic polymer that dissolves in an acidic environment and forms gels. Its properties depend on the degree of deacetylation and molecular weight. It is a bioactive compound with antibacterial and film-forming properties that allow to increase the regenerative capacity of the skin. Moreover, it is biodegradable, biocompatible, non-toxic, and stable. In this research, chitosan was combined with mandelic and lactobionic acids which are characterized by biological activity and low toxicity. This combination not only has a positive effect on the chitosan solubility, but it also allows to obtain new biomaterials whose positive features of the base ingredients are enhanced by their synergistic effect. The obtained hydrogels were assessed regarding the interaction of chitosan and hydroxy acid molecules, and the stability of the resulting structures was examined. The research was performed by using rheological methods and IR spectroscopy.

Chitosan hydrogels made with mandelic acid are characterized by higher viscosity values, as compared to hydrogels containing lactobionic acid. The samples of the obtained hydrogels stored for 7 days showed no signs of degradation and their viscosity values were constantly increasing, which proves the ongoing process of creating new bonds between hydroxy acid molecules and chitosan chains. After this time, the hydrogels with mandelic acid revealed higher viscosity values in comparison to hydrogels made with lactobionic acid. Based on the obtained IR spectra, the shifts of the characteristic chitosan bands as a result of interaction with the tested hydroxy acids were analyzed.

Keywords: chitosan, lactobionic acid, mandelic acid, rheology, FTIR spectra

[Engineering of Biomaterials 161 (2021) 2-7]

doi:10.34821/eng.biomat.161.2021.2-7



Copyright © 2021 by the authors. Some rights reserved. Except otherwise noted, this work is licensed under <https://creativecommons.org/licenses/by/4.0>

Introduction

In recent years, there has been a growing trend in tissue engineering to use natural biopolymers from various sources. These include, for example, proteins, lipids and polysaccharides which can be obtained, among others, from marine organisms. They are represented by collagen (so-called marine), chitin and its derivative - chitosan. These compounds have found application in biomaterials due to their biocompatibility, non-toxicity and biodegradability. Stable hydrogels are formed through the process of self-assembly or as a result of chemical or physical cross-linking, which helps to restore natural tissues [1,2].

Chitosan (FIG. 1) is produced by chemical or enzymatic deacetylation of chitin. It dissolves only in acidic solutions at a pH lower than 6 due to the presence of intermolecular hydrogen bonds that prevent the dissolution of chitosan in water or in organic solvents [1,3]. As a result of the protonation of the amino groups in the acidic environment, chitosan behaves like a cationic polymer. The presence of positively charged amino groups is closely associated with the antimicrobial activity of this compound. These groups interact with the negatively charged cell wall surface of the microorganism. Then, the membrane is damaged and the internal structures of the pathogen are destroyed. In addition, there is another mechanism of the antimicrobial action of chitosan. It is related to its ability to chelate metal ions necessary for the proper functioning of microorganisms, and thus chitosan contributes to their death [4-8]. Of all the known natural polymers, chitosan has the highest chelating capacity [2].

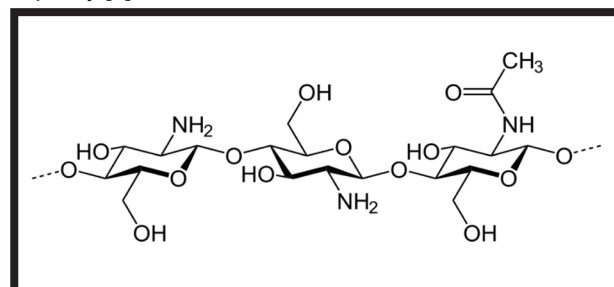


FIG. 1. Structure of a chitosan molecule.

The positively charged chitosan molecule adheres to other negatively charged surfaces, including mucous membranes. This can facilitate drug delivery by various routes - oral, nasal, and direct application to the eye [2].

The degree of deacetylation and molecular weight have a large influence on the physicochemical properties and bioactivity of chitosan. There are three types of chitosan: low molecular weight (LMW), medium molecular weight (MMW) and high molecular weight (HMW). Chitosan with the low molecular weight and high deacetylation has been shown to have better antibacterial properties and better solubility than the one with the high molecular weight and low deacetylation [6-9].

Chitosan has the ability to increase the influx of phagocytic cells to the infection site and it affects the proliferation of fibroblasts. Additionally, it is able to aggregate platelets at the site of damaged tissues. This shortens the bleeding in the initial stage of wound healing and contributes to the formation of a fibrin clot. Chitosan also stimulates the production of cytokines and activates macrophages and neutrophils, which results in the cleansing of a wound. Literature data indicate that the polymer contributes to the formation of granulation tissue and contributes to the correct course of epithelization.

In addition, it stimulates angiogenesis and reduces scar visibility. Chitosan is also an inhibitor of the metalloproteinase 2 (MMP-2) present in skin fibroblasts and hydrolysing type IV collagen. The inhibition of this process facilitates the correct reconstruction of damaged tissues in the case of chronic wounds [4,10-14].

All the previously mentioned properties of chitosan make it a very desirable component of biomaterials, and the positive effects of its use have been confirmed by many scientific studies. Chitosan can take various forms in biomedical materials, for example hydrogels [15], nanofibers [16], micro-particles [17], nanoparticles [18] or scaffolds [19]. Chitosan biomaterials have been extensively studied for the treatment of wounds of various etiologies in the creation of dressing materials, including burn wounds and pressure ulcers. In combination with collagen, a nanocomposite membrane was created that promotes wound healing and induces cell migration and proliferation [20]. Chitosan-alginate nanofibers act in a similar way [21-23]. Fibers made of carboxymethyl chitosan and polyvinyl alcohol constitute the scaffold in the skin regeneration process [16,24]. Chitosan hydrogels, showing similar physical properties to the extracellular matrix, have become a promising dressing material enabling diffusion and stimulation of cell proliferation. They also have the appropriate sorption capacity and antibacterial properties. In the form of hydrogels, chitosan is combined with silver nanoparticles or minocycline which belongs to antibiotics. It is also a promising material for use in carriers for the delivery of analgesic or anti-cancer drugs to improve their performance [4,10,15].

Chitosan has also been studied in the engineering of bone, cartilage and nervous tissues. It is part of special scaffolds (in combination with nanoceramics - hydroxyapatite, silicon dioxide or bioactive glass-ceramics) that support regeneration, increase cell adhesion, proliferation and differentiation. Such scaffolds induce only a minimal foreign body response. The compound was also tested in combination with polycaprolactone or whitlockite in an *in vivo* experiment to repair skull defects. Such combination increase the activity of the compounds and improve the mechanical properties of the structures. Chitosan-based hydrogels can be also administered by intra-articular injection to cause the regeneration of cartilage tissue. There have been also experiments on the effects of chitosan scaffolds on nervous tissue. In the studies carried out on rats, it was possible to obtain positive effects in the regeneration of nerves [1,4,10,25].

Moreover, chitosan biocomposites can be used in dentistry. They effectively counteract bacteria that are responsible for the formation of caries and periodontal diseases. Chitosan can also be an element influencing the differentiation of pulp stem cells. Moreover, it is a potential replacement for some antibiotics that work against drug-resistant bacteria [1].

Research on the use of chitosan in biomaterials focuses on finding ingredients that will work synergistically. A good example are hydroxy acids (for example, lactobionic acid and mandelic acid), since chitosan is soluble only in acidic solutions. These two acids are characterized by good biological activity and low toxicity, therefore they create the required acidic environment to dissolve the polymer [26-28].

Lactobionic acid (4-O- β -D-galactopyranosyl-D-gluconic acid, $C_{12}H_{22}O_{12}$) is a derivative of lactose. It belongs to the group of polyhydroxy acids, its pKa is 3.8. A molecule of lactobionic acid is a combination of gluconic acid with galactose (FIG. 2) with a molecular weight of 358.3 g/mol.

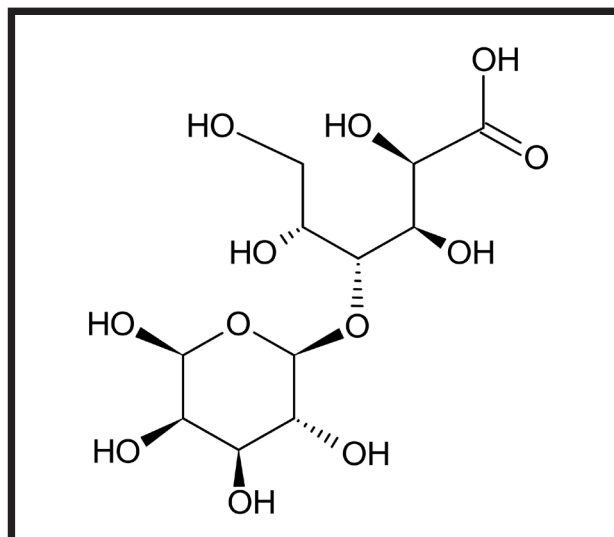


FIG. 2. Structural formula of lactobionic acid.

Due to the presence of 8 hydroxyl groups in the molecule, this compound has very good hygroscopic properties and high water solubility. There is another carboxyl group in the molecule that can react with functional groups of other substances (for example, with an amino group). Mostly it is produced by chemical synthesis, in the process of lactose oxidation or by enzymatic or microbiological biosynthesis. Another method of preparation is wet catalytic oxidation and electrochemical catalysis of lactose. However, this process results in the by-products of these reactions and higher costs. Lactobionic acid in combination with chitosan forms stable gels [29-31].

In the last decade, interest in lactobionic acid has increased in fields, such as pharmacy, medicine, cosmetology, the chemical and food industries [31,33-36]. It is also increasing in popularity as a bioactive molecule providing an excellent platform for the synthesis of biocompatible and biodegradable biomaterials, tissue engineering scaffolds and drug delivery carriers [26,32,34].

Studies on the lactobionic acid combined with copper or with micro-capsuled chitosan were conducted regarding the treatment of hepatocellular carcinoma in the liver. The obtained results are the basis for carriers used in drug delivery systems to a specific organ. These compounds have been used as substrates in the synthesis of radiopharmaceuticals that target liver cell imaging receptors. Researchers have also suggested the suitability of lactobionic acid to design nanofiber scaffolds supporting the regeneration of damaged nerves [26,31-33].

Lactobionic acid has also found application in the production of pharmaceutical products and antibiotics. It has a strong antibacterial effect, inter alia, against *Staphylococcus aureus* and *Staphylococcus epidermidis*. Thanks to this, it may be used in antimicrobial drugs that are not antibiotics. Lactobionic acid is also added to solutions intended for the preservation and storage of transplantable organs. In the pharmaceutical industry, it is currently used as a counterion for the intravenous administration of erythromycin and in mineral supplementation to minimize irritation during the therapy. In addition, it can be used as a component to form nanoparticles. It acts as a stabilizer in pharmaceuticals containing low-stability ingredients. Such a wide application of lactobionic acid is related to the fact that it is non-irritating, non-toxic, biocompatible and biodegradable [31,32,34].

Lactobionic acid, when applied externally, has the ability to stimulate fibroblasts to produce collagen and elastin. It accelerates the wound healing process, has strong antioxidant properties, and strengthens the epidermal barrier function. It has been shown to stop the production of hydroxyl radicals as a result of its chelating properties and to inhibit the action of metalloproteinase enzymes - enzymes that contribute to skin photoaging. Free radicals are also responsible for causing skin cancer and skin autoimmune diseases. Lactobionic acid prevents the formation of wrinkles, sagging skin, dilatation, and cracking of capillaries [31,35,36].

Mandelic acid (2-phenyl-2-hydroxyacetic acid, $C_8H_8O_3$) belongs to the group of optically active α -hydroxy acids, which contain an aromatic ring in their structure (FIG. 3). Its pKa value is 3.4. The structure of the acid allows it to be dissolved in both polar and non-polar solvents. It is well soluble in ethyl alcohol, isopropyl alcohol, and partially in water and fats. The natural source of mandelic acid are almonds, apricots, and cherries. It can be obtained as a result of the hydrolysis of the bitter almond extract [37,38].

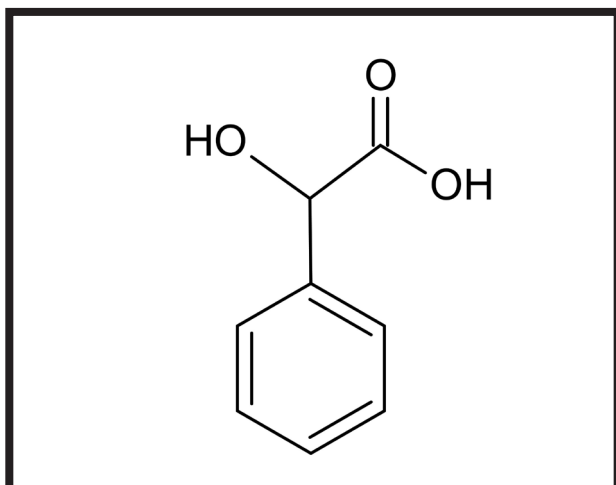


FIG. 3. Structural formula of mandelic acid.

Mandelic acid exists in the form of two enantiomers, S and R, which determine its properties. (R)-mandelic acid is widely used as an intermediate product for the production of semi-synthetic cephalosporins, penicillin and anticancer agents, while (S)-mandelic acid is a component of intermediates used in the production of pharmaceuticals. Both enantiomers are effective resolving agents which are used in the resolution of racemic amines and alcohols [39,40].

Mandelic acid is used in many medical and peri-medical fields, including dermatology, pharmacy, and cosmetology. It usually occurs in a racemic form. It has keratolytic properties that regulate the work of sebaceous glands, therefore it supports the therapy of acne or excessive actinic keratosis. It gives good results in combating discoloration of various etiologies (for example freckles, acne scars or drug discoloration). That is why, it is widely used in cosmetology. Due to the relatively large size of the molecule, it is absorbed slowly through the skin, thus showing a low irritating potential, acting gently and safely, but slower than other α -hydroxy acids [38,41].

The described compound is distinguished by a strong disinfecting and antibacterial effect. In an acidic environment, it has a bacteriostatic and bactericidal effect on, among others, strains of *Staphylococcus aureus* or *Escherichia coli*. This property allows it to be used in the case of pharmaceuticals, antibiotics or external agents [41].

The properties of lactobionic and mandelic acids allow their use in combination with chitosan in biomedical materials. These acids will beneficially interact with the polymer, enhancing its biological activity and creating a suitable acidic environment for its dissolution. The safety of their use will be maintained because the combined compounds will not cause irritation and will be non-toxic, biocompatible, and biodegradable.

The aim of the presented work was to investigate the physicochemical and rheological properties of chitosan hydrogels obtained by dissolving low molecular weight chitosan in solutions of mandelic or lactobionic acids. In addition to rheological studies, infrared spectroscopy was also performed.

Materials and Methods

Materials

Chitosan powder (low molecular weight, degree of deacetylation DD = 78%, $M_v = 1.4 \times 10^6$ g/mol [42]), lactobionic and mandelic acids were obtained from Merck (Poznań, Poland) and used without further purification.

Preparation of chitosan gels

Hydrogels were prepared by dissolving chitosan (2.6% w/v) in 30 ml of aqueous solutions of mandelic acid and lactobionic acid. The content of hydroxyacids was 0.002 mol. The samples were mixed for an hour at the temperature of 25°C on a magnetic stirrer until clear solutions were obtained.

Viscosity measurements

After 24 hours of incubation, viscosity measurements were taken at the temperature of $25 \pm 0.1^\circ\text{C}$ in the range of the shear rate from 0.1 s^{-1} to 35 s^{-1} . The measurements were repeated 5 times per conditions. The rotational viscometer SMART series (Fungilab, Warsaw, Poland) and a set of appropriate spindles were used for the measurements.

FT-IR analysis

The structure of chitosan, mandelic and lactobionic acids as well as the interaction between them were confirmed by infrared spectroscopy, using Nicolet iS10 device (Shimadzu, Kyoto, Japan). All the spectra were recorded by absorption mode at 4 cm^{-1} intervals and 64-times scanning. After the 24 h incubation, the obtained hydrogels were poured in the amount of 25 g into square Petri dishes (10 cm x 10 cm) and allowed to dry. The finished films were carefully removed from the plates and submitted to the FT-IR analysis. The measurements were repeated 3 times per conditions on the different parts of the film.

Results and Discussions

In the presented work, the viscosity characteristics of chitosan solutions obtained by dissolving low-molecular-weight chitosan in solutions of lactobionic acid and mandelic acid were compared, and the changes of these characteristics over time were analyzed. The rheological tests were performed after 24, 48, 72, 168 and 312 hours from the preparation of the samples. The samples were stored at 8°C. Before the measurements, the samples were thermostated to 25°C.

As a result of the rheological studies, the dependence of dynamic viscosity on the shear rate (viscosity curves) was obtained. It allowed to conclude that hydrogels based on chitosan and mandelic acid are characterized by higher viscosity values, as compared to those containing lactobionic acid.

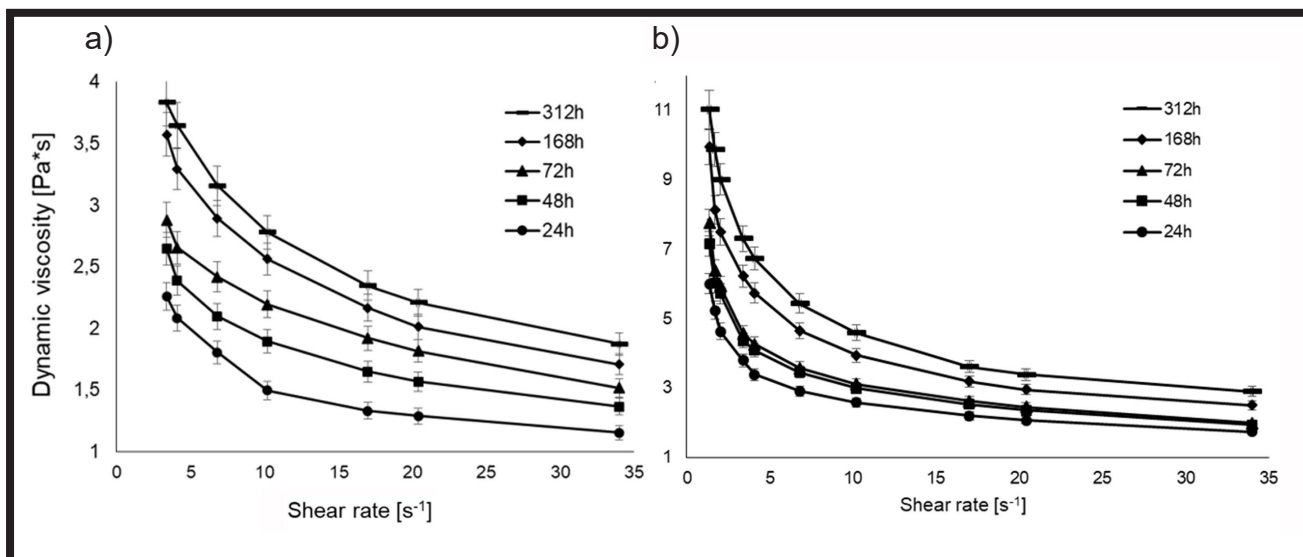


FIG. 4. Comparison of dynamic viscosity of chitosan gel with lactobionic acid (a) and mandelic acid (b) depending on the time.

On the basis of the obtained viscosity curves (FIG. 4), it can be concluded that chitosan gels, characterized by an identical molar ratio of chitosan and acid, prepared with mandelic acid show more than twice higher viscosity than those made with lactobionic acid. The difference in the viscosity parameters of chitosan gels with lactobionic acid and mandelic acid results from the difference in the structure of acids, their strength and the way the polymer interacts with the acid molecules. The interaction of mandelic acid with the chitosan molecule will form an ionic bond between the protonated amino group of chitosan and the dissociated carboxyl group. At the same time, the hydroxyl group of the acid can join another chitosan amino group, but due to the short distance between the carboxyl and hydroxyl groups, most likely belonging to another chitosan chain. The compact flat aryl ring located between the chitosan chains allows them to be closer to each other and interact with the formation of hydrogen bonds, which also contributes to the viscosity increase. The following processes improve the viscosity of the gel formed with mandelic acid gel more than that with lactobionic acid.

Lactobionic acid will interact with the chitosan chains in a similar way, linking the dissociated carboxyl group with the protonated amino group of chitosan, and the hydroxyl groups of the polyhydroxy acid will also form associations with the amino groups of both the same chitosan chain and different chains. It can be assumed that hydroxyl groups of lactobionic acid characterized by different acidity interact with the polymer amino groups, resulting in the formation of association complexes. In this way, the lactobionic acid molecule can bind to the amino groups of both a specific chitosan chain, causing its conformation, and other chains, which increases the resulting hydrogel viscosity. However, it can be assumed that these types of bonds will be characterized by lower stability, which in the case of using lactobionic acid results in lower values of dynamic viscosity. A more spatially expanded lactobionic acid molecule causes a looser arrangement of chitosan chains in relation to each other and thus the lower viscosity of the obtained gels. In the case of mandelic acid, the bonds are formed by the interaction of the carboxyl and hydroxyl groups with the amino groups of different chitosan chains, linking them with each other and thus contributing to the higher viscosity than in the case of lactobionic acid.

By examining the changes in viscosity characteristics up to 312 hours of observation, it was found that the viscosity of the systems for both lactobionic and mandelic acid continued to increase (FIG. 4). This fact can only be explained by the formation of new bonds between chitosan and acid molecules. Both mandelic acid (pKa 3.4) and lactobionic acid (pKa 3.8) are weak acids. However, the protonation of amino groups in chitosan in an acidic environment will result in a shift of the equilibrium towards the increasing acid dissociation. This, in turn, creates more bonds between acid molecules and chitosan chains and contributes to the higher viscosity of the obtained gels. The data available in the literature on the interaction of chitosan with hydroxy acids is very limited [43-45], and there is even less information on viscosity tests of such systems.

In order to consider the interaction of individual functional groups of compounds forming the biopolymer, spectroscopic examinations in the infrared range are conducted. In this study, the interactions between the functional groups of chitosan and lactobionic or mandelic acids were tested by Fourier transform infrared spectroscopy.

The FTIR spectra of chitosan, lactobionic acid and mandelic acid are shown in FIG. 5. The characteristic peak at 3280 cm^{-1} (Amide A), 2860 cm^{-1} (C-H), 1645 cm^{-1} (Amide I), 1540 cm^{-1} (Amide II) and 1025 cm^{-1} (C-O-C) are usually observed for chitosan samples. The axial deformation, or stretching bands, for lactobionic acid were observed at: 3320 cm^{-1} ($\text{OH}_{\text{alcohol}}$), 2885 cm^{-1} (C-H), 870 cm^{-1} (ring vibration), 1110 cm^{-1} and 1220 cm^{-1} (C-O), 1730 cm^{-1} ($\text{C}=\text{O}_{\text{acid}}$). The bands of the lactobionic acid sample corresponded to the ones known from the literature [46]. The following peaks were observed for a crystalline sample of mandelic acid: 3400 cm^{-1} (OH), a wide band in the range $3030\text{-}2700\text{ cm}^{-1}$ ($\text{C-H}_{\text{stretch}}$), 1720 cm^{-1} ($\text{C}=\text{O}_{\text{acid}}$), $1500\text{-}490\text{ cm}^{-1}$ (mainly ring deformations and o-, m-, p-CH bends). These bands of mandelic acid also correspond to the data found in the literature [47].

In the FTIR spectra of films made of chitosan with lactobionic or mandelic acid, we can observe changes in both the location of the observed peaks and their intensity (FIG. 5). After the formation of bonds between chitosan and acids, we do not observe peaks corresponding to $\text{C}=\text{O}_{\text{acid}}$, also the OH peak (3400 cm^{-1}) for mandelic acid disappears, and the corresponding peak for lactobionic acid loses its intensity.

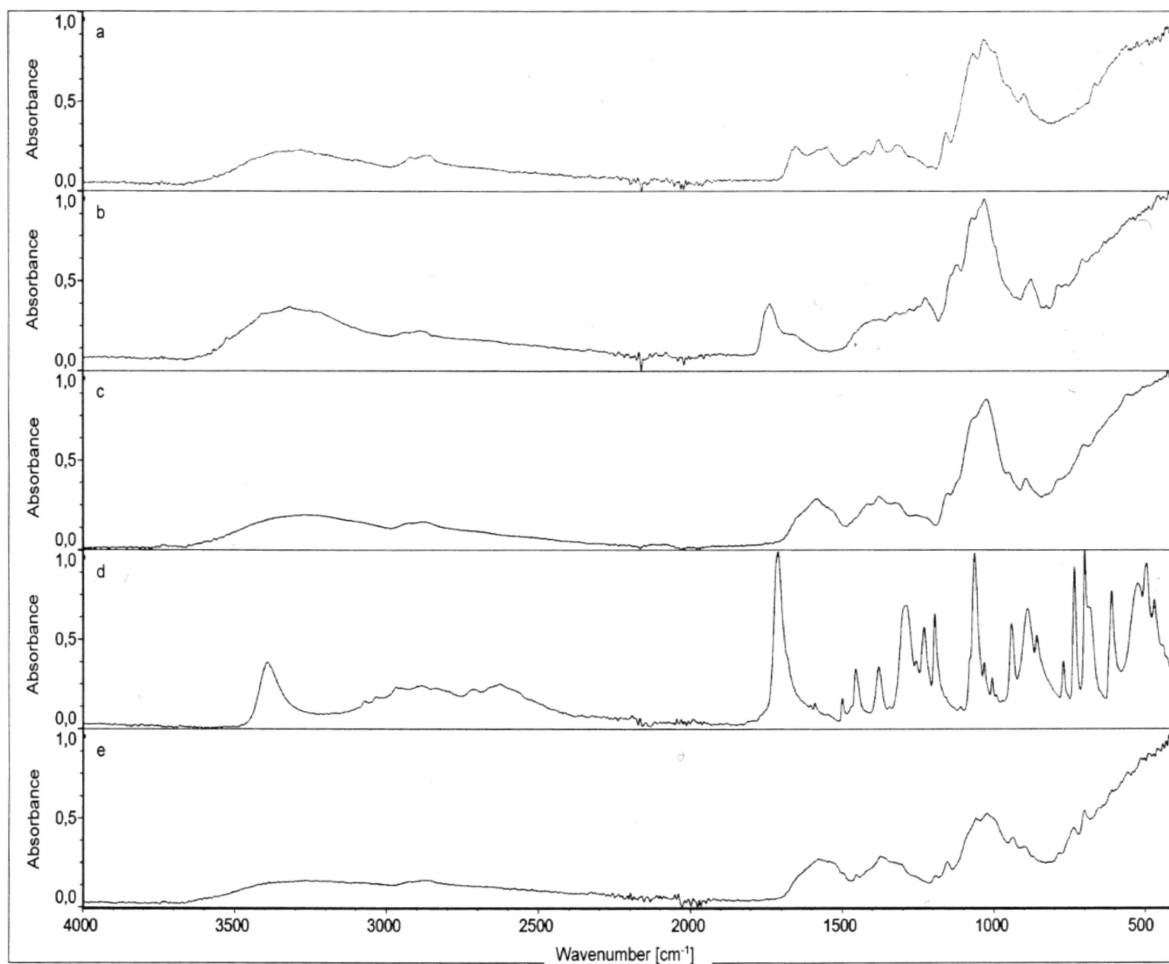


FIG. 5. FTIR spectra of chitosan (a), lactobionic acid (b), mandelic acid (d) and chitosan hydrogels with lactobionic acid (c) and mandelic acid (e).

On the other hand, in the spectrum of both films, new peaks that may belong to the protonated amino group are observed, with the intensity of these peaks for lactobionic acid being slightly higher. The comparison of the bands for pure compounds and the obtained hydrogels shows the participation not only of the carboxyl group of the hydroxy acid but also of the hydroxyl groups that form bonds between chitosan and acids

Conclusions

The viscosity values of chitosan hydrogels (2.6% w/v) based on lactobionic or mandelic acids (each acid content was 0.002 mol) as components of potential application in biomaterials were investigated. The rotational viscometer SMART series (Fungilab, Poland) was used. Viscosity measurements were made at the temperature of $25 \pm 0.1^\circ\text{C}$ in the range of the shear rate from 0.1 s^{-1} to 35 s^{-1} . The structure of chitosan, mandelic acid and lactobionic acid as well as the interactions between them were confirmed by infrared spectroscopy using Nicolet iS10 device (Shimadzu, Japan).

The viscosities of hydrogels depending on the structure of the hydroxy acid and the change of hydrogel viscosity with time were analyzed. It was observed that chitosan hydrogels prepared on the basis of mandelic acid showed higher dynamic viscosity than those prepared on the basis of lactobionic acid. It was proved that the dynamic viscosity of the prepared samples for both acids in the time range up to 312 hours was characterized by an upward trend.

These phenomena can be explained by the difference in the interaction mechanisms of chitosan and acid molecules, depending on their structure and the difference in acid strength.

Based on the FTIR spectra, it was proved that both carboxyl and hydroxyl groups were involved in the interaction between chitosan and hydroxy acid molecules. The viscosity increased over time due to the progressive process of protonization of the amino groups resulting from the progressive dissociation of hydroxy acids and the increasing number of bonds between chitosan and hydroxy acids.

A combination of the unique properties of chitosan with the bioactivity of hydroxy acids, such as lactobionic acid and mandelic acid, will be useful in the preparation of a biomaterial for wound healing dressing.

Acknowledgements

Financial support from a student mini-grant obtained from Collegium Medicum, Nicolaus Copernicus University is gratefully acknowledged.

ORCID iDs

O. Zavyalova: <https://orcid.org/0000-0002-0098-1633>
 S. Gajewska: <https://orcid.org/0000-0002-1152-1501>
 D. Dąbrowska-Wisłocka: <https://orcid.org/0000-0002-9675-2500>
 A. Sionkowska: <https://orcid.org/0000-0002-1551-2725>

References

- [1] Wan M., Qin W., Lei C., et al.: Biomaterials from the sea: Future building blocks for biomedical applications. *Bioactive Materials* 6 (2021) 4255-4285.
- [2] Joyce K., Fabra G.T., Bozkurt Y., et al.: Bioactive potential of natural biomaterials: identification, retention and assessment of biological properties. *Signal Transduction and Targeted Therapy* 6 (2021) 122.
- [3] Mucha M.: Chitozan: wszechstronny polimer ze źródeł odnawialnych. WNT, Warszawa 2010.
- [4] Kędzierska M., Miłowska K.: Zastosowanie biomateriałów na bazie chitozanu w leczeniu trudno gojących się ran. *Postępy Higieny i Medycyny Doświadczalnej* 73 (2019) 768-781.
- [5] Jayakumar R., Menon D., Manzoor K.: Biomedical applications of chitin and chitosan based - A short review. *Carbohydrate Polymers* 82 (2010) 227-232.
- [6] Matica A., Menghiu G., Ostafe V.: Antibacterial properties of chitin and chitosans. *New Frontiers in Chemistry* 26 (2017) 39-54.
- [7] Moeini A., Pedram P., Makvandi P., et al.: Wound healing and antimicrobial effect of active secondary metabolites in chitosan-based wound dressings: A review. *Carbohydrate Polymers* 233 (2020) 115839.
- [8] Bano I., Arshad M., Yasin T., et al.: Chitosan: A potential biopolymer for wound management. *International Journal of Biological Macromolecules* 102 (2017) 380-383.
- [9] Baroudi A., Garcia-Payo C., Khayet M.: Structural, Mechanical, and Transport Properties of Electron Beam-Irradiated Chitosan Membranes at Different Doses. *Polymers* 10 (2018) 1-23.
- [10] Ostrowska-Czubenko J., Pieróg M., Gierszewska M.: Modyfikacja chitozanu – krótki przegląd. *Wiadomości chemiczne* 70 (2016), 657-679.
- [11] Wiśniewska-Wrona M., El Fray M.: Właściwości fizykochemiczne i funkcjonalne biokompozytów polimerowych. *Polimery* 64 (2019) 23-33.
- [12] Azuma K., Izumi R., Osaki T., et al.: Chitin, Chitosan, and Its Derivatives for Wound Healing: Old and New Materials. *Journal of Functional Biomaterials* 6 (2015) 104-142.
- [13] Mazurek P., Kuliński S., Gosk J.: Możliwości wykorzystania chityny i chitozanu w leczeniu ran. *Polimery w medycynie* 43 (2013) 297-302.
- [14] Sakthiguru N., Sithique A.: Fabrication of bioinspired chitosan/gelatin/allantoin biocomposite film for wound dressing application. *International Journal of Biological Macromolecules* 152 (2020) 873-883.
- [15] Rodríguez-Rodríguez R., Espinosa-Andrews H., Velasquillo-Martínez C.: Composite hydrogels based on gelatin, chitosan and polyvinyl alcohol to biomedical applications: a review. *International Journal of Polymeric Materials and Polymeric Biomaterials* 69 (2018) 1-20.
- [16] Pouranvari S., Ebrahimi F., Javadi G., et al.: Chemical cross-linking of chitosan/polyvinyl Alcohol electrospun nanofibers. *Materials and technology* 50 (2016) 663-666.
- [17] Udrea L. E., Hritcu D., Popa M. I. et al.: Preparation and characterization of polyvinyl alcohol-chitosan biocompatible magnetic microparticles. *Journal of Magnetism and Magnetic Materials* 323 (2011) 7-13.
- [18] Sionkowska A., Walczak M., Michalska-Sionkowska M.: Preparation and characterization of collagen/chitosan composites with silver nanoparticles. *Polymer Composites* 41 (2019).
- [19] Kozłowska J., Stachowiak N., Sionkowska A.: Preparation and characterization of collagen/chitosan poly (ethylene glycol)/nanohydroxyapatite composite scaffolds. *Polymers for Advanced Technologies* 30 (2018) 799-803.
- [20] Sionkowska A., Kaczmarek B., Stalinska J., et al.: Biological Properties of Chitosan/Collagen Composites. *Key Engineering Materials* 587 (2013) 205-210.
- [21] Kaczmarek B., Sionkowska A., Stojkowska J.: Characterization of scaffolds based on chitosan and collagen with glycosaminoglycans and sodium alginate addition. *Polymer Testing* 68 (2018) 229-232.
- [22] Kyzioł A., Mazgala A., Michna J., et al.: Preparation and characterization of alginate/chitosan formulations for ciprofloxacin-controlled delivery. *Journal of Biomaterials Applications* 32 (2017) 162-174.
- [23] Gåserød O., Smidsrød O., Skjåk-Braek G.: Microcapsules of alginate-chitosan - I - A quantitative study of the interaction between alginate and chitosan. *Biomaterials* 19 (1998) 1815-25.
- [24] Mahato K.K., Yadav I., Singh M., et al.: Polyvinyl alcohol / chitosan lactate composite hydrogel for controlled drug delivery. *Materials Research Express* 6 (2019).
- [25] de Sousa Víctor R., Marcelo da Cunha Santos A., Viana de Sousa B. et al.: A Review on Chitosan's Uses as Biomaterial: Tissue Engineering, Drug Delivery Systems and Cancer Treatment. *Materials* 13 (2020) 4995.
- [26] Zhang J., Li C., Xue Z.-Y.: Fabrication of lactobionic-loaded chitosan microcapsules as potential drug carriers targeting the liver. *Acta Biomaterialia* 7 (2011) 1665-1673.
- [27] Ni. P., Li R., Ye S., et al.: Lactobionic acid-modified chitosan thermosensitive hydrogels that lift lesions and promote repair in endoscopic submucosal dissection. *Carbohydrate Polymers* 263 (2021) 118001.
- [28] Lin W.J., Chen T.D., Liu C.-W.: Synthesis and characterization of lactobionic acid grafted pegylated chitosan and nanoparticle complex application. *Polymer* 50 (2009) 4166-4174.
- [29] Gutiérrez L.-F., Hamoudi S., Belkacemi K.: Lactobionic acid: A high value-added lactose derivative for food and pharmaceutical applications. *International Dairy Journal* 26 (2012) 103-111.
- [30] Bisinella R.Z.B., Ribeiro J.C.B. et al.: Some instrumental methods applied in food chemistry to characterise lactulose and lactobionic acid. *Food Chemistry* 220 (2017) 295-298.
- [31] Alonso S., Rendueles M., Diaz M.: Bio-production of lactobionic acid: Current status, applications and future prospects. *Biotechnology Advances* 31 (2013) 1275-1291.
- [32] Alonso S.: Exploiting the bioengineering versatility of lactobionic acid in targeted nanosystems and biomaterials. *Journal of Controlled Release* 287 (2018) 216-234.
- [33] Zhao X., Li X., Huang X., et al.: Development of lactobionic acid conjugated-copper chelators as anticancer candidates for hepatocellular carcinoma. *Arabian Journal of Chemistry* 14 (2021) 103241.
- [34] Wojciechowska A., Klewicki R., Klewicka E.: The potential of new bionic acids as prebiotics and antimicrobials. *LWT - Food Science and Technology* 125 (2020) 109246.
- [35] Tasic-Kostov M., Pavlovic D., Lukic M., et al.: Lactobionic acid as antioxidant and moisturizing active in alkyl polyglucoside-based topical emulsions: the colloidal structure, stability and efficacy evaluation. *International Journal of Cosmetic Science* 34 (2012) 424-434.
- [36] Tang S.-Ch., Yang J.-H.: Dual Effects of Alpha-Hydroxy Acids on the Skin. *Molecules* 23 (2018) 863.
- [37] Yarolimek M., Kennermur J.: Exploration of mandelic acid-based polymethacrylates: Synthesis, properties, and stereochemical effects. *Journal of Polymer Science* 58 (2020) 3349-3357.
- [38] Jankowiak W., Imielski W., Janeba-Bartoszewicz E.: Zastosowanie kwasu migdałowego w peelingu kosmetycznym. *Kosmetologia Estetyczna* 5 (2016) 57-60.
- [39] Gao B., Chen L., Li Y.: Preparation of surface imprinted material of single enantiomer of mandelic acid with a new surface imprinting technique and study on its chiral recognition and resolution properties. *Journal of Chromatography A* 1443 (2016) 10-20.
- [40] Wang P., Yang J., Jiang L., et al.: A bi-enzymatic system for efficient enantioselective bioconversion of racemic mandelic acid. *Journal of Molecular Catalysis B: Enzymatic* 94 (2013) 47-50.
- [41] Lebedowska A.: Kwas migdałowy jako popularny składnik peelingów chemicznych. *Aesthetica* 5 (2014) 66-68.
- [42] Lewandowska K., Sionkowska A., et al.: Characterization of chitosan composites with various clays. *International Journal of Biological Macromolecules* 65 (2014) 534-541.
- [43] Retno A.L., Dwi S., Mudasir M.: Preparation of Citric Acid Crosslinked Chitosan/Poly(Vinyl Alcohol) Blend Membranes for Creatinine Transport. *Indonesian Journal of Chemistry* 16 (2016) 144-150.
- [44] Kählig H., Hasanovic A., et al.: Chitosan-glycolic acid: a possible matrix for progesterone delivery into skin. *Drug Development and Industrial Pharmacy* 35 (2009) 997-1002.
- [45] Lin W.J., Chen T.D., Liu C.W.: Synthesis and characterization of lactobionic acid grafted pegylated chitosan and nanoparticle complex application. *Polymer* 50 (2009) 4166-4174.
- [46] Bisinella R., Ribejro J., et al.: Some instrumental methods applied in food chemistry to characterise lactulose and lactobionic acid. *Food Chemistry* 220 (2017) 295-298.
- [47] Badawi H., Förner W.: Analysis of the infrared and Raman spectra of phenylacetic acid and mandelic (2-hydroxy-2-phenylacetic) acid. *Spectrochimica Acta Part A* 78 (2011) 1162-1167.

NEW DESIGN OF PATIENT-SPECIFIC, ANTIMICROBIAL BIOACTIVE FINGER IMPLANTS FOR DURABLE FUNCTIONAL RECONSTRUCTION AFTER AMPUTATION

MARCIN DYNER¹ , ADAM BYRSKI² ,
ROMAN MAJOR^{2*} , MACIEJ GAWLIKOWSKI³ ,
KATARZYNA KASPERKIEWICZ⁴ , JUERGEN M.
LACKNER⁵ , ANETA DYNER⁶ , BOGUSŁAW MAJOR² 

¹ FACULTY OF SCIENCE AND TECHNOLOGY,
JAN DLUGOSZ UNIVERSITY IN CZESTOCHOWA,
ARMII KRAJOWEJ AV, 13/15,
42-200 CZESTOCHOWA, POLAND

² INSTITUTE OF METALLURGY AND MATERIALS SCIENCE,
POLISH ACADEMY OF SCIENCES,
REYMONTA ST. 25, 30-059 KRAKOW, POLAND

³ SILESIA UNIVERSITY OF TECHNOLOGY,
FACULTY OF BIOMEDICAL ENGINEERING,
DEPARTMENT OF BIOSENSORS AND PROCESSING
OF BIOMEDICAL SIGNALS,
ROOSEVELT STR. 40, ZABRZE, POLAND

⁴ UNIVERSITY OF SILESIA IN KATOWICE,
FACULTY OF NATURAL SCIENCES, INSTITUTE OF BIOLOGY,
BIOTECHNOLOGY AND ENVIRONMENTAL PROTECTION,
JAGIELLOŃSKA ST. 28, 40-032 KATOWICE, POLAND

⁵ JOANNEUM RESEARCH FORSCHUNGSGES.M.B.H.,
INSTITUTE OF SURFACE TECHNOLOGIES AND PHOTONICS,
FUNCTIONAL SURFACES,
LEOBNER STRASSE 94, 8712 NIKLASDORF, AUSTRIA

⁶ MEDICAL INSTRUMENTS FACTORY
CHIRMED MARCIN DYNER,
MSTOWSKA ST. 8A, 42-240 RUDNIKI, POLAND

*E-MAIL: R.MAJOR@IMIM.PL

Abstract

The absence of even a single finger results in a major impairment in the hand function (precise grasping, grip power), therefore significantly affecting the social and professional life of victims who are frequently young people. Finger amputation is a surgical treatment for ~69.000 patients in the EU after traumatic injury, in which replantation microsurgery fails due to the severity of tissue damage. The surgical reconstruction is currently possible only via autograft transplantation, e.g. a toe-to-hand transfer, thus leading to foot impairment. Some motion functional restoration is also possible using a bone-anchored silicone prosthesis but without the sense revalidation.

Our current research focuses on alternatives for surgical reconstruction by means of novel patient-specific, durable, biomimetic, bioactive and antibacterial implants for reconstructing lost bone and joints. The implant design – and the improved micro(neuro) surgery (beyond the project) – will consist in the fast successful rehabilitation, including the soft-tissue related mobility, the implantation of state-of-the-art nerve conduits as well as the aesthetic appearance.

Key issues for the long-term functionality of the biomaterial-based reconstruction of hard tissue are based on surgical demands, such as: (1) perfect integration of a bone-substituting metal with the surrounding bone tissue (a) with no signs of loosening due to stress shielding at the interface and (b) enhanced with protective activity against bacterial inflammation (antimicrobial properties and formation of vascularized bone tissue (ossification)) even months to years after the injury; (2) biomimetic finger joints based on non-wearing materials without ossification meant to prevent the loss of the motion function.

Keywords: finger implant, thin coatings, microstructure, cytotoxicity, microbiology

[*Engineering of Biomaterials* 161 (2021) 8-14]

doi:10.34821/eng.biomat.161.2021.8-14



Copyright © 2021 by the authors. Some rights reserved.
Except otherwise noted, this work is licensed under
<https://creativecommons.org/licenses/by/4.0>

Introduction

Optimal treatment after accidental finger amputation

A traumatic finger (digit) amputation is the most common type of highly severe injury of the upper extremities [1-3]. The hand and digital amputations account for ~69.000 visits to emergency departments in the EU (~45.000 in the US) [4,5]. The absence of even a single finger (especially the thumb, ~15.000 patients/year in EU) results in major impairments in the hand function, i.e. the inability to perform more precise manoeuvres and engage in specific tasks and the decreased power of the grip, causing social inhibition and inadequate adaptation to society [6-8]. The multiple finger loss only increases the disadvantageous impact on life and work (i.e. productivity and income) [9].

Victims of severe finger injuries are usually young and in their prime income earning years [9]. Thus, choosing an appropriate treatment can bring substantial economic effects, not only to trauma patients but also to the lives of their families and society. Medically, an amputation is a relatively inexpensive and uneventful procedure, but in addition to the motion and sensing disability, the persistent pain is problematic. Although costly and microsurgically challenging, the gold standard for preserving the hand mechanics is replantation, offering substantial functional and aesthetic benefits [10-13]. It is performed in ~24% of all cases in Austria, 22% in EU28, 14% in the US and 29% in Japan with generally higher prevalence in the case of amputation of >2 digits. The procedure requires a long rehabilitation period and can result in functional deficits owing to persistent finger stiffness and limited sensation [14-17]. However, if the microsurgical reconstruction fails (14% of cases [14] or replantation is not an option due to the injury severity (e.g. after crushing without a clean-cut) (~38% of total cases), techniques such as finger pollicisation or a toe-to-hand transfer can also offer a good reconstructive alternative [18]. Some finger functionality is preserved with external silicone prostheses [19-21], if they connect to bone-anchored implants (in contrast to a snap prosthesis providing only aesthetic function) [21,22]. However, anchoring is rarely used due to the high risks of bacterial infection, prosthesis extrusion and osseous absorption of the phalangeal stump [23,24].

Since immunogenicity risks prevent the use of any allografts and xenografts, the autologous reconstruction from patient's own donor tissue without the loss of other extremities (e.g. toes) is currently increasingly considered as a future alternative, especially for patients after the loss of the thumb or 2 and more fingers (estimated 15,000 cases/year in EU). While the autologous connective tissue, tendons and skin transfer from donor sites, including the vascularization, is considered a (micro-)surgical standard, the main challenge is the hybridization of this surgical approach with implants. The problematic issues consist in:

(1) the reconstruction of the finger bone segments as well as joints. When the available donor sites of bone are either strongly limited (e.g. from the iliac crest) or missing (for joints), it is necessary to apply bone- and joint-substitute materials. However, finger-bone-substituting implants (for reconstructing phalanx and metacarpal bones) have to be patient-tailored to match the length and anchoring geometry to the existing bone/joints. Finger-joint implants are currently available only for replacing arthritic joints. They are not suitable for the combination with any bone-substituting implants and have strong functionality limitations due to the material ossification (metal or polymer).

(2) the reduction of germ count and minimizing the rate of post-traumatic hand bone infections caused by bacteria introduced during the injury or the medical-surgical treatment (nosocomial, partly multi-resistant nosocomial *Staph. aureus* & *epidermidis*, *E. coli*, *Pseudomonas*) [25].

(3) the tactile function restoration: the loss of sensation of e.g. both digital nerves of the thumb (even if the motion is still possible without the amputation) equals 20% loss of the hand function [26]. Tactile sensibility can be restored by various neurovascular flap techniques [27] and a number of nerve guidance conduits and nerve protectant wraps approved by the US Food and Drug Administration (FDA) for clinical use in the peripheral nerve repair [28].

General demands for autologous tissue & implant scaffold based reconstruction

In order to reconstruct the finger using a durable, patient-tailored, biomimetic and bioactive implant (the R&D target of the fingerIMPLANT project, bullet points 1&2 from above), special focus must be laid on the highly complex reconstruction of motion, i.e. using structural implants (materials in demanded shape) for finger bone and joint reconstruction.

Soft-tissue related mobility, implantation of state-of-the-art nerve conduits and aesthetic appearance (bullet point 3) are mainly a task for the post-project clinical studies on adapting available microsurgical techniques.

Based on the consortium experience, the necessary patient-specific implants for reconstruction of bones, joints and tactile function must mandatorily be:

(1) non-cytotoxic and biocompatible for the long-term use, i.e. initially anti-microbial and bioactive to provide the proper bone neoformation,

(2) patient-tailored to the size and shape of the digital defect ("finger length"), the elasticity of surrounding bone at the interface to the existing bone in order to prevent stress shielding and degradation of the surrounding bone, and comparatively manageable for the surgeon,

(3) mechanically robust to provide sufficient strength against physical forces *in vivo* (similarly to the normal finger and hand motion).

The long-term surgical experience with tissue engineering, bone-substitute materials and artificial joints shows that any implant concept without metal- or ceramic-based, durable high-strength materials have failed in osteosynthesis and functional reconstruction due to heavy loads and a high number of load cycles (movements) affecting the extremities. Consequently, the following demands arise for the biometric design of bone and joint reconstruction:

Patient-tailored bone reconstruction implants

An excellent, patient-tailored adaptation of the implant to the patient-specific dimensional demands of the phalanx and metacarpal bones as well as providing fast axonal regrowth is essential to minimize the process of learning the new grasp, adding to an already huge burden of accepting the reconstructed extremity. Furthermore, arthroplasty in small bones generally shows that the implant stiffness has to be adapted to the natural bone stiffness in the areas of direct contact (anchoring sites) because the elasticity differences will result in the bone degradation caused by stress-shielding and therefore the implant loosening.

The most important characteristics that the implant must fulfil are:

(1) The response to loading similar to natural bone at the anchoring sites (Young's modulus (E) 25-30 GPa (ISO 6892-1) to prevent stress shielding by using design methodology for 4D printing (3D shape + directionally-optimized stiffness by cellular inner structure).

(2) Long-term mechanical and corrosion durability - tensile testing ISO 6892-1:2016: (tensile strength >800 MPa), fatigue limit (106 cycles, >400 MPa).

Tribologically and chemically durable artificial ceramic joint implants

The state-of-the-art silicone or PEEK polymer-based finger joint implants for arthritic joint replacement generally fail mechanically after 2-4 years [29-34], the CoCr or pyrolytic carbon joints fail due to loosening, ossification or wear after the similarly long use [35-38]. The demands are, thus, as follows:

(1) the non-osteoconductive material to prevent the osteoblast adhesion and ossification

(2) the highly smooth (Ra<10 nm) surface after the polishing post-treatment, both high hardness (>1200 HV) & toughness >6 MPa m^{0.5} for the minimized wear rate (<0.1 mm³/107 cycles, modified ISO 14242 test)) and the reduced anchoring sites of osteoblasts (start of ossification)

(3) the high-quality material for biomedical applications (bulk density >3.94 g/cm³, grain size <4.5 μm, flexural strength >400 MPa) (ASTM F603-12)

Thin bioresorbable, osteoconductive and antimicrobial coatings on metal implants

Generally, full metal-based bone-substitute implants impede the optimal interaction with the surrounding tissue due to the tissue capsula formation and the risk of persistent inflammation caused by the bacteria biofilm. So, to improve the implant/tissue interaction, metal implants may be coated with bioresorbable osteoconductive materials (like hydroxyapatite (HAp)) to enable leaching necessary osteoinductive ions dedicated for the faster bone neoformation during the slow dissolution in body fluids. This widely-used (e.g. for joint arthroplasty) safe approach of an *in vivo* bioreactor inside the patient's body, instead of the *ex vivo* cell cultivation with the excessive manipulation of cells, is mandatory for tissue engineering due to the rigid regulations.

Finally, such an approach leads to the key benefit i.e. the formation of a natural-like bone layer. However, state-of-the-art industrial coating technologies do not fulfil the demands of low-temperature processing to prevent distortion of small implant sizes. Further, materials like HAp are insufficient to protect deep wounds and bone destruction from the enormous risk of bacterial colonization in the cases of finger traumas. In spite of the initial antibiotic therapy, inflammation may occur even some weeks past the injury and/or the final reconstruction surgery in less vascularized regions with low blood supply, such as the implant surface. This constricts further bone formation and results in implant rejection if the emergency anti-biotic treatment is inefficient. Based on the joint substitute know-how, the medical demands for a coating technique at low temperatures (<120°C) are the following:

(1) the biodegradation of osteoinductive HAp within 15-20 weeks as a basis for neoformation of a thin layer (500 - max. 1000 µm) of natural-like vascularized cortical bone on the implant

(2) the local anti-microbial protection during these 15-20 weeks of the HAp biodegradation phase after implantation (decrease of *Staph. aureus* & *epidermidis*, *E. coli*, *Pseudomonas* from 1E5 to <1E0 /ml in 24 h, ISO 22196 test conditions) to prevent the biofilm formation and the finger implant loss.

The main objective of the study was to design and manufacture a prototype finger implant.

Materials and Methods

The research and development of the optimized, biomimetic implant based on finite element modelling is the origin of developing (i) high-elastic Ti-15Mo-5Zr-3Al scaffolds with partly bionic cellular structures as bone substitutes and (ii) ultra-tough, smooth, complex 3D-shaped ZrO₂-Al₂O₃ ceramic joint substitutes for additive manufacturing by adapted selected laser melting (SLM) and lithography-based ceramic manufacturing (LCM), respectively.

Microstructure analysis

The surface morphology was examined with scanning electron microscopy (SEM). Prior to the imaging step, the samples were coated with a gold thin film to prevent the tissue surface charging. The visualization was performed by FEI Versa 3D FEG SEM (FEI, Poland), with the 5.0 kV – 10.0 kV acceleration voltage and the electron beam current of 4.0 nA.

The study was performed from the cross-section using transmission electron microscopy (TEM) Tecnai G2 F20 (200 kV). The thin films for the TEM analysis were prepared by the focused ion beam technique (FIB) using gallium ions by the device QUANTA 200 3D Dual Beam.

Cytotoxicity

The task addresses issues of the possible cytotoxic effects of biomaterials, i.e. the fibroblasts necrosis in relation to the control group tested on the Ti6Al4V alloy with confirmed biocompatibility. The cytotoxicity test of samples was performed by the indirect method according to ISO 10993-5 on murine fibroblasts (L929 ATCC). The potential cytotoxic effect was determined according to the ISO 10993-5:2009 standards. Twenty-three samples measuring 1.5 cm² were placed in confluent mouse fibroblast (L929; ATCC) cultures (about 5x10⁵ cells) and incubated for 48 h at 37°C.

Then the cells were stained with propidium iodide (PI). The images were taken with the Axio Imager confocal microscope equipped with a camera and quantified using Axio-Vision 4.6 (Carl Zeiss MicroImaging). A statistical analysis (two-way ANOVA and Tukey post hoc test, P value smaller than 0.05 was considered as significant – Statistica 10.0 PL) was performed on three replicates from each treatment.

The number of live and necrotic cells was assessed by confocal microscopy using the propidium iodide (PI) marker MitoTracker green which stains active mitochondria. This marker localizes the mitochondria independently of the mitochondrial membrane potential. The propidium iodide test is one of the more commonly used methods for cytotoxicity testing. To label mitochondria, cells are incubated with MitoTracker® probes which passively diffuse across the plasma membrane and accumulate in the active mitochondria. After labelling their mitochondria, the cells can be treated with an aldehyde-based fixative for the samples that require fixation to allow further sample processing. Some MitoTracker® probes are also preserved after permeabilisation with certain detergents during subsequent processing steps (e.g. Immunocytochemistry or *in situ* hybridisation). Propidium iodide penetrates into the cell only when the continuity of the cell membrane is breached. Upon entering the cytoplasm, it labels nucleic acids and upon excitation with green light, it turns the nucleus of the necrotic cell red.

Microbiology

The antimicrobial activity contact test was based on ISO 22196:2007(E). *Escherichia coli* strain ATCC 8739 (Gram-negative) and *Staphylococcus aureus* strain 6538P (gram-positive) were used, as recommended in the norm. The obtained results were visualized as antibacterial activity index (R) which represents the difference between the number of viable bacteria recovered from both untreated and treated specimens. To analyze the microbiological properties of the coatings according to ISO 22196, the samples were inoculated with a bacterial suspension of the units that formed a colony of approximately 2.5 x 10⁵ – 1.0 x 10⁶ / ml (cfu). *Staphylococcus aureus* (ATCC® 6538P™) and *E. coli* (ATCC® 8739™) strains were selected for the study. The samples were incubated for 24 h at 95% relative humidity and at 37°C. To determine the initial number of bacteria, the microorganisms were counted after having been applied to the biomaterial and quickly washed away from its surface.

Results and Discussions

The concept of the implant

The suggested implant design is presented in FIG. 1. The image shows the bone part and the joint part.

The material topography and microstructure

The surface topography images were obtained by scanning electron microscopy at an accelerating voltage of 2 kV, using a secondary electron detector. One of the images was taken with the table tilted to 52 degrees to obtain a three-dimensional image (FIG. 2). The microstructural tests were performed on the reference flat samples, not on the implant. The surface, shown in FIG. 2, corresponds to the surface dedicated to the bone fixation.

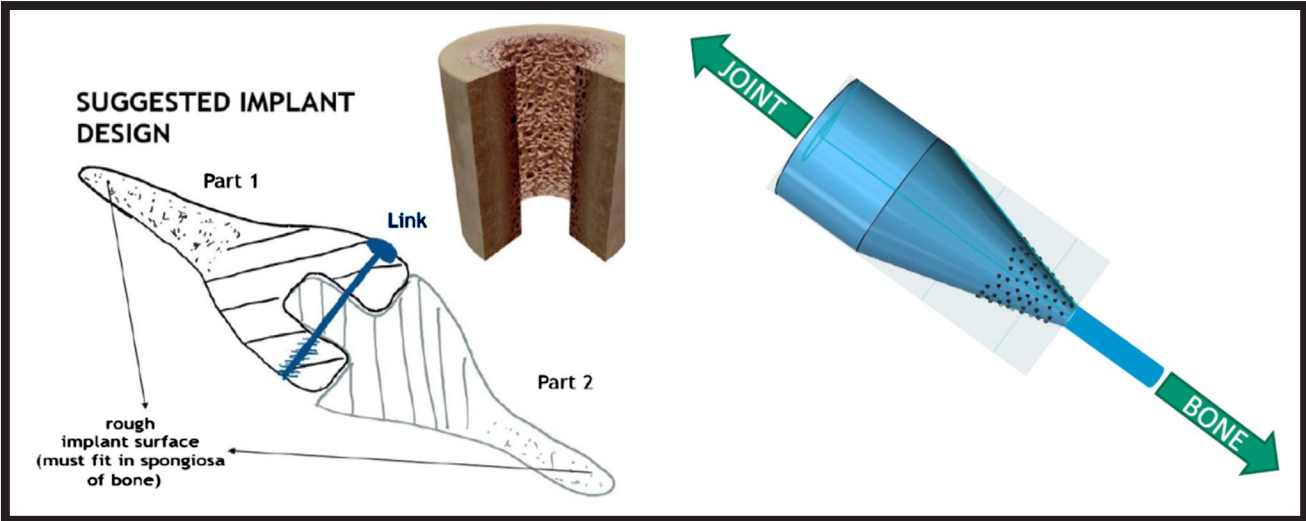


FIG. 1. The concept of the design: A - the suggested implant design, B - the concept of the implant-bone connection.

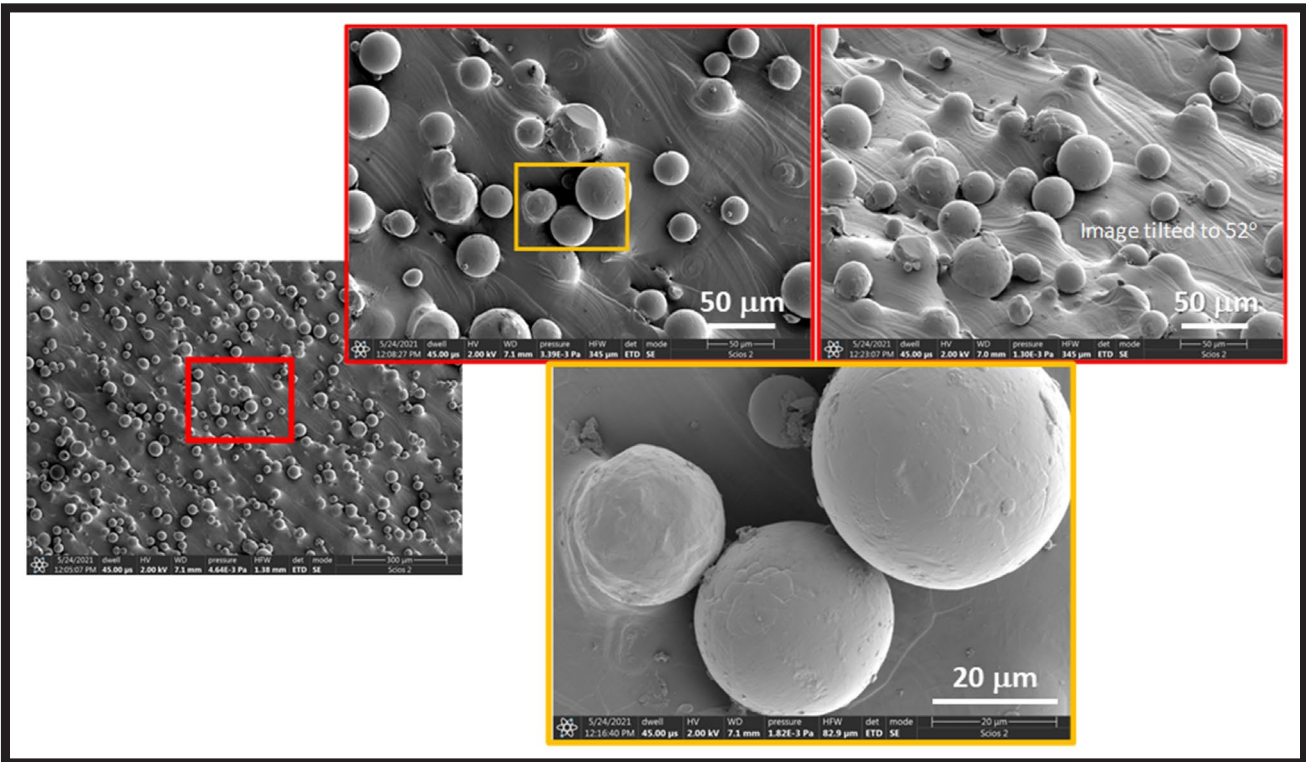


FIG. 2. SEM topography analysis of the materials intended for implants.

The detailed microstructural characterization was carried out using transmission electron microscopy on the cross-section (FIG. 3). A thin film was cut from the boundary between the substrate and the sphere. The sphere region showed the columnar growth of crystallites in the direction perpendicular to the sphere surface. Twinning was also shown, due to the tendency for twinning in hcp structures.

In order to better visualize the crystallites in the sphere area, the microstructural characterization was carried out in the dark field of observation from a selected diffraction reflector (FIG. 4).

Twinning is one of the main deformation modes in hexagonal close-packed (HCP) materials, and it has a great influence on mechanical properties.

The direct cytotoxic effect

The cytotoxic effect of the materials on the cells was determined according to the 10993 standard of the direct cytotoxicity analysis of materials. The tests were carried out using molecular probes of the mitotracker type to test the level of mitochondrial activation and propidium iodide which labels necrotic cells (FIG. 5).

The graph was developed by the colocalisation function. The colocalization analysis is performed on a pixel by pixel basis. Every pixel in the image is plotted in the scatter diagram based on its intensity level from each channel. The colour in the scatterplot represents the number of pixels that are plotted in that region. In this example, the green intensity is shown on the x-axis and the red intensity is shown on the y-axis.

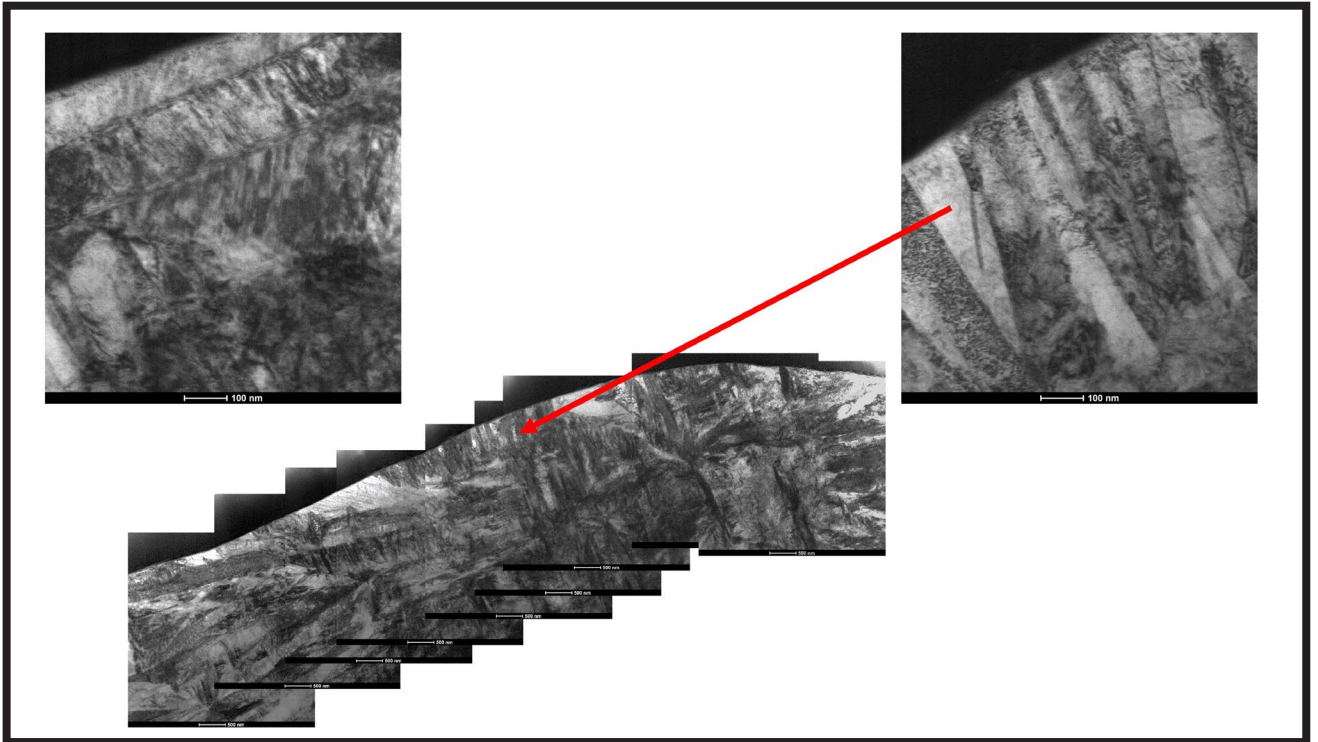


FIG. 3. TEM micrograph of the HCP structure of the coating.

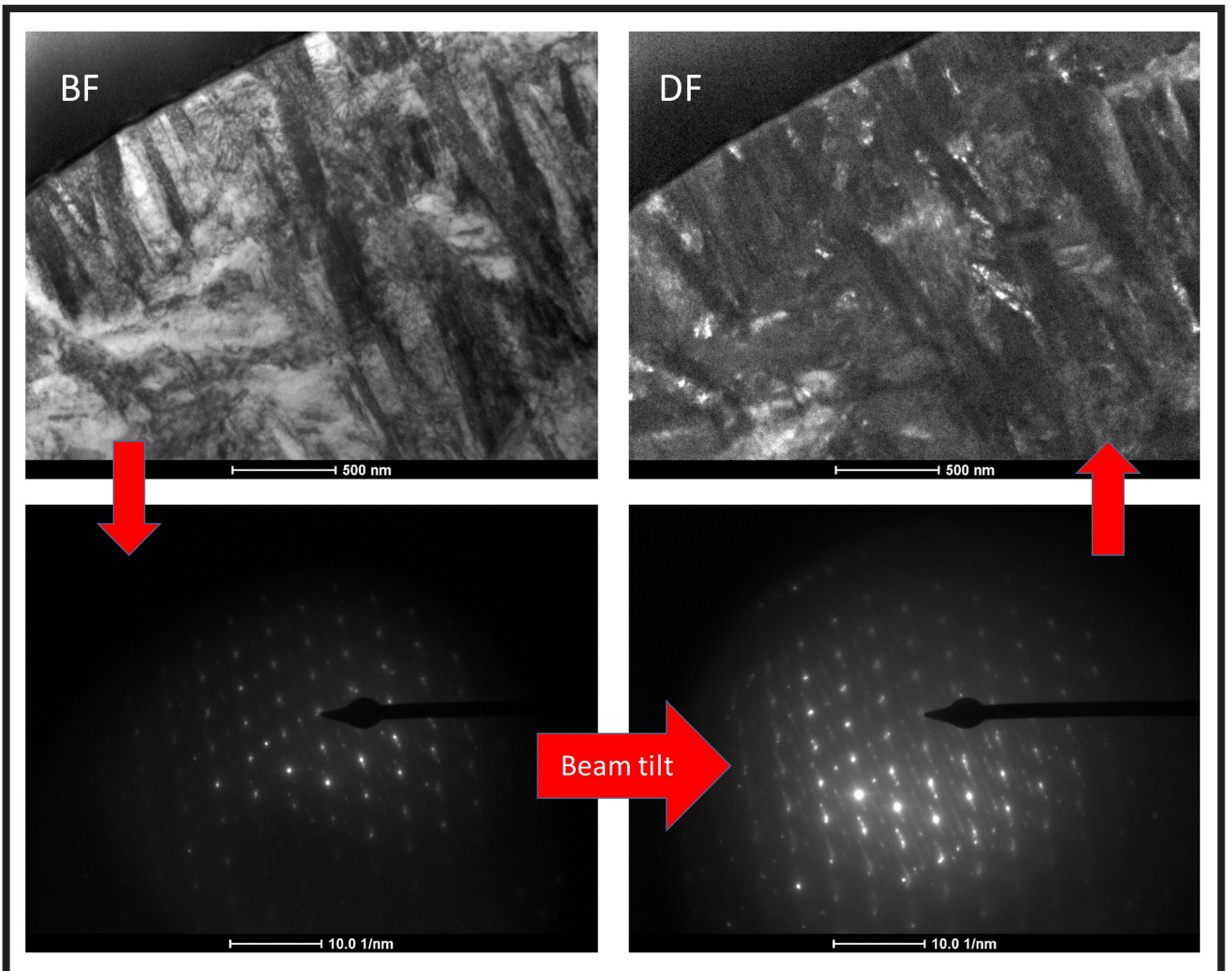


FIG. 4. Bright field image of the coating microstructure.

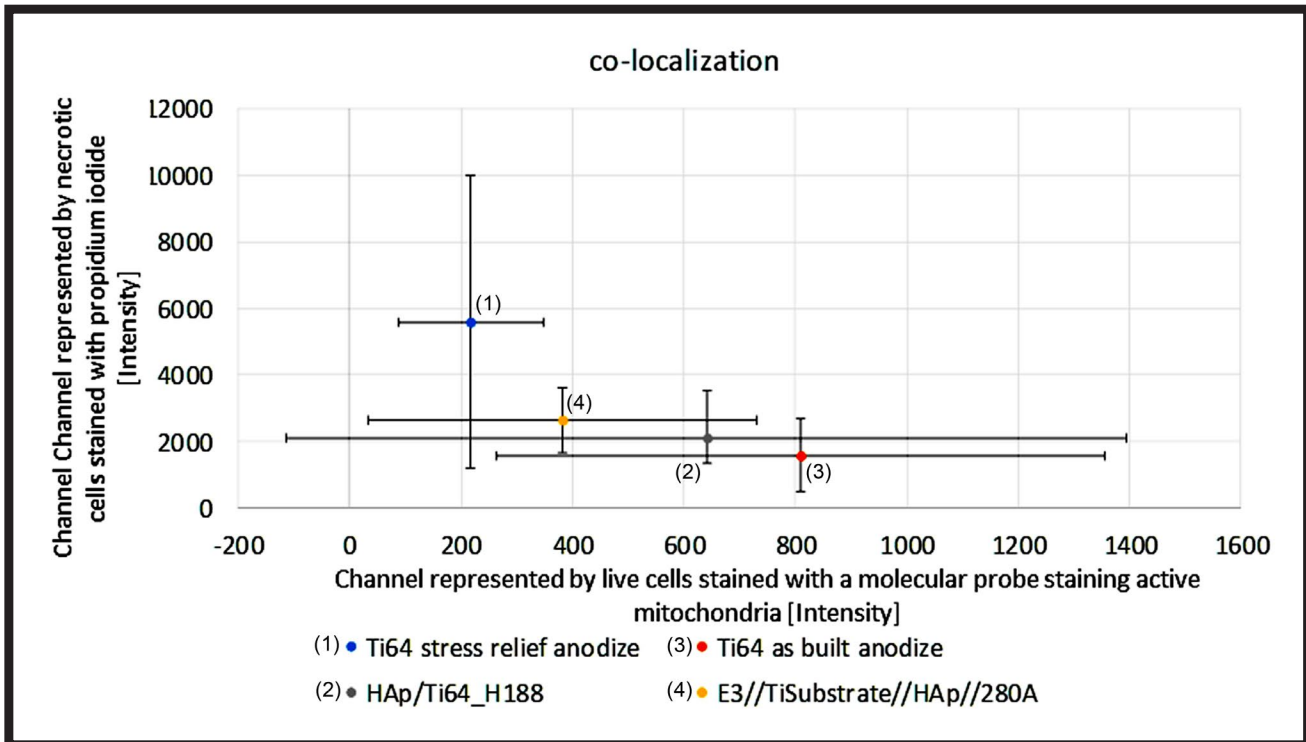


FIG. 5. Cytotoxic effect of the tested materials on the cells.

TABLE 1. The antimicrobial activity assumption.

Biomaterial	Antibacterial activity R against:	
	<i>E. coli</i>	<i>S. aureus</i>
HAp/Ti64_H188	6.5	2.2
E3//TiSubstrate//HAp//280A	2.6	2.3

The microbiological effect

The antimicrobial activity value is presented in TABLE 1. The obtained results were visualized as antibacterial activity index (R) which represents the difference between the number of viable bacteria recovered from both the untreated and treated specimens. The material yields antibacterial properties if the calculated R value is greater than 2 (orders of magnitude). The higher the R index is, the better the antibacterial properties are.

Conclusions

The materials dedicated to the finger reconstruction were tested on the nanoscale and the microstructure was optimized for the proper overgrowth with the tissue. The microbiological tests showed good properties, i.e. antimicrobial properties for both the metallic substrate material and the hydroxyapatite-coated material. This is a very important characteristic of implant materials. The cytotoxicity tests did not show conclusive properties. A high probability of the necrotic comet formation and a large statistical scatter were observed, which may still indicate the low repeatability of the results. This feature will be refined in the near future, taking into account the positive microbiological aspects.

Acknowledgements

This research was financially supported by the Polish National Centre of Research and Development (Grant no. fingerIMPLANT M-ERA.NET2/2019/7/2020, "Patient-specific, anti-microbial bioactive finger implants for durable functional reconstruction after amputation").

ORCID iDs

M. Dyrner: <https://orcid.org/0000-0002-9943-6335>
 A. Byrski: <https://orcid.org/0000-0003-1152-5964>
 R. Major: <https://orcid.org/0000-0003-3809-1908>
 M. Gawlikowski: <https://orcid.org/0000-0002-6526-2656>
 K. Kasperkiewicz: <https://orcid.org/0000-0002-9851-790X>
 J.M. Lackner: <https://orcid.org/0000-0003-3931-232X>
 A. Dyrner: <https://orcid.org/0000-0001-7387-7178>
 B. Major: <https://orcid.org/0000-0001-9471-1230>

References

- [1] J.P. Leigh, S.B. Markovitz, M. Fahs, C. Shin, P.J. Landrigan: Occupational Injury and Illness in the United States. *Arch. Intern. Med.* 157 (1997) 1557.
- [2] K.C. Chung, M.J. Shauver: Table Saw Injuries. *Plast. Reconstr. Surg.* 132 (2013) 777e-783e.
- [3] E. Davis Sears, K.C. Chung: Replantation of Finger Avulsion Injuries: A Systematic Review of Survival and Functional Outcomes. *J. Hand Surg. Am.* 36 (2011) 686-694.
- [4] E. Mahmoudi, P.R. Swiatek, K.C. Chung, J.Z. Ayanian: Racial Variation in Treatment of Traumatic Finger/Thumb Amputation. *Plast. Reconstr. Surg.* 137 (2016) 576e-585e.
- [5] J.M. Conn, J.L. Annest, G.W. Ryan, D.S. Budnitz: Non-Work-Related Finger Amputations in the United States, 2001-2002. *Ann. Emerg. Med.* 45 (2005) 630-635.
- [6] C.J. Goodacre, G. Bernal, K. Rungcharassaeng, J.Y. Kan: Clinical complications with implants and implant prostheses. *J. Prosthet. Dent.* 90 (2003) 121-132.
- [7] N. Shanmuganathan, M.U. Maheswari, V. Anandkumar, T.V. Padmanabhan, S. Swarup, A.H. Jibrán: Aesthetic finger prosthesis. *J. Indian Prosthodont. Soc.* 11 (2011) 232-237.
- [8] C. Aydin, S. Karakoca, H. Yilmaz: Implant-retained digital prostheses with custom-designed attachments: A clinical report. *J. Prosthet. Dent.* 97 (2007) 191-195.
- [9] D. Boyle, D. Parker, C. Larson, L. Pessoa-Brandão: Nature, incidence, and cause of work-related amputations in Minnesota. *Am. J. Ind. Med.* 37 (2000) 542-550. <http://www.ncbi.nlm.nih.gov/pubmed/10723048> (accessed May 28, 2019).
- [10] G.M. Buncke, H.J. Buncke, C.K. Lee: Great Toe-to-Thumb Microvascular Transplantation After Traumatic Amputation. *Hand Clin.* 23 (2007) 105-115.
- [11] H. Wang: Secondary surgery after digit replantation: Its incidence and sequence. *Microsurgery.* 22 (2002) 57-61.
- [12] R.A. Bueno, B. Battiston, D. Ciclamini, P. Titolo, B. Panero, P. Tos: Replantation. *Clin. Plast. Surg.* 41 (2014) 385-395.
- [13] L. Jazayeri, J.Q. Klausner, J. Chang: Distal Digital Replantation. *Plast. Reconstr. Surg.* 132 (2013) 1207-1217.
- [14] S.J. Sebastin, K.C. Chung: A Systematic Review of the Outcomes of Replantation of Distal Digital Amputation. *Plast. Reconstr. Surg.* 128 (2011) 723-737.
- [15] D. Fufa, R. Calfee, L. Wall, W. Zeng, C. Goldfarb: Digit Replantation: Experience of two U.S. academic level-I trauma centers. *J. Bone Jt. Surg.* 95 (2013) 2127-2134.
- [16] M.J. Shauver, T. Nishizuka, H. Hirata, K.C. Chung: Traumatic Finger Amputation Treatment Preference among Hand Surgeons in the United States and Japan. *Plast. Reconstr. Surg.* 137 (2016) 1193-1202.
- [17] R.D. Goldner, M. V. Stevanovic, J.A. Nunley, J.R. Urbaniak: Digital replantation at the level of the distal interphalangeal joint and the distal phalanx. *J. Hand Surg. Am.* 14 (1989) 214-220.
- [18] M.A. Pet, J.H. Ko, N.B. Vedder: Reconstruction of the Traumatized Thumb. *Plast. Reconstr. Surg.* 134 (2014) 1235-1245.
- [19] V. Cervelli, D.-J. Bottini, A. Arpino, M. Grimaldi, M. Rogliani, P. Gentile: Bone-anchored implant in cosmetic finger reconstruction. *Ann. Chir. Plast. Esthétique.* 53 (2008) 365-367.
- [20] B. Yeshwante, N. Parasrampur, N. Baig: Prosthetic Rehabilitation of an Amputated finger. *IOSR J. Dent. Med. Sci.* 13 (2014) 10-17.
- [21] N. Yadav, P. Chand, S.K. Jurel: Rehabilitation of single finger amputation with customized silicone prosthesis. *Natl. J. Maxillofac. Surg.* 7 (2016) 89-91.
- [22] S. Sharma, G. Chand Baid, V. Lath, N. Gupta, S. Chandra Pankaj: Rehabilitation of an amputated finger - a case report. *J. Evol. Med. Dent. Sci.* 6 (2017) 744-748.
- [23] A. Sierakowski, C. Watts, K. Thomas, D. Elliot: Long-term outcomes of osseointegrated digital prostheses for proximal amputations. *J. Hand Surg. European Vol.* 36 (2011) 116-125.
- [24] P. Doppen, M. Solomons, S. Kritzinger: Osseointegrated Finger Prostheses. *J. Hand Surg. European Vol.* 34 (2009) 29-34.
- [25] E. Drampalos, H.R. Mohammad, C. Kosmidis, M. Balal, J. Wong, A. Pillai: Single stage treatment of diabetic calcaneal osteomyelitis with an absorbable gentamicin-loaded calcium sulphate/hydroxyapatite biocomposite: The Silo technique. *Foot.* 34 (2018) 40-44.
- [26] A.B. Swanson, C.G. Hagert, G.D. Swanson: Evaluation of impairment of hand function. *J. Hand Surg. Am.* 8 (1983) 709-722.
- [27] L.-W. Lok, W.-L. Chan, Y.-K. Lau: Functional Outcomes of Antegrade Homodigital Neurovascular Island Flaps for Fingertip Amputation. *J. Hand Surg. Asian-Pacific Vol.* 22 (2017) 39-45.
- [28] S. Kehoe, X.F. Zhang, D. Boyd: FDA approved guidance conduits and wraps for peripheral nerve injury: A review of materials and efficacy. *Injury.* 43 (2012) 553-572.

ASSESSMENT OF THE PROPERTIES OF HAp MICROPOWDERS AFTER ION EXCHANGE PROCESS IN SILVER NITRATE SOLUTION

MARTA GŁUSZEK¹ , ZUZANNA ŚWIRSKA¹ ,
WITOLD KACZOROWSKI^{1*} , BARTŁOMIEJ
JANUSZEWICZ¹ , MACIEJ WRONIAK² 

¹ INSTITUTE OF MATERIALS SCIENCE AND ENGINEERING,
LODZ UNIVERSITY OF TECHNOLOGY,
STEFANOWSKIEGO 1/15, 90-924 LODZ, POLAND

² CLINICAL DEPARTMENT OF ORTHOPEDIC-TRAUMATIC,
ONCOLOGICAL AND RECONSTRUCTIVE SURGERY,
ST. BARBARA SPECIALIZED REGIONAL HOSPITAL No. 5,
SOSNOWIEC, PLAC MEDYKÓW 1,
41-200 SOSNOWIEC, POLAND

*E-MAIL: WITOLD.KACZOROWSKI@P.LODZ.PL

Abstract

Bioceramic materials, such as hydroxyapatite (HAp), are characterized by high biocompatibility in the presence of tissues and body fluids without causing toxic or allergic reactions. Hydroxyapatite, due to its similarity to structures found in bones, is used both in the form of powders, e.g. as additives to bone cements, and implants coatings. However, this material is not characterized by antimicrobial properties, therefore attempts are made to improve its properties by introducing additional elements into the hydroxyapatite structure. Thanks to HAp's high ion-exchange ability, silver can be introduced into its structure. The calcium ions present in the HAp structure can be easily replaced by silver ions to create a material endowed with high biocompatibility and antibacterial properties. The presented study is based on the analysis of the morphology of the modified powders via scanning electron microscopy (SEM), their chemical composition via X-ray energy dispersive spectroscopy (EDS) and chemical structure via X-ray diffraction (XRD) and Raman spectroscopy. The powders obtained through the ion exchange were mixtures of silver phosphates Ag_3PO_4 and HAp. The highest silver content was found in the sample modified with a 1M concentration of $AgNO_3$ in the aqueous solution. It was also determined that the annealing of the obtained powders under vacuum at 800°C resulted in the formation of metallic silver and a change in the structure of HAp to β -TCP.

Keywords: hydroxyapatite, ion exchange, silver nitrate (V), annealing, XRD, Raman spectroscopy

[Engineering of Biomaterials 161 (2021) 15-20]

doi:10.34821/eng.biomat.161.2021.15-20



Copyright © 2021 by the authors. Some rights reserved.
Except otherwise noted, this work is licensed under
<https://creativecommons.org/licenses/by/4.0>

Introduction

Hydroxyapatite $Ca_{10}(PO_4)_6(OH)_2$ belongs to the group of apatite minerals with a Ca/P molar ratio of 1.667. It has a hexagonal structure tightly packed with atoms, therefore this compound has a rather high density - 3.16 g/cm³ [1,2]. Hydroxyapatite is a biologically active material whose chemical and phase composition is similar to that of human bone. The biggest advantage of hydroxyapatite is its porosity which gives the possibility of bone tissue ingrowth [3,4]. In addition, the mere presence of calcium and phosphorus ions at the interface between the ceramic and the bone tissue enables faster bonding between the bone and the implant [5-7]. HAp dissolves relatively well in acids and poorly in water. It is characterized by a high ion exchange capacity [8-10]. One way to modify hydroxyapatite is to incorporate silver into its structure [11-13]. W. Chen et al. [14] and M. Rai et al. [15] showed that HAp is an optimal material for introducing silver ions. The Ca^{2+} ions present in the HAp structure can be easily replaced by Ag^+ ions, creating a material with high biocompatibility and antibacterial properties. The antibacterial properties of silver have been used in many fields of medicine for years, which is evidenced by the wide range of preparations available on the market [16]. Since ancient times silver has been used in the treatment of extensive wounds and burns [17,18]. Silver in small amounts has low toxicity to human cells, high thermal stability, and low volatility with prolonged action, indicating biofilm inhibitory properties [19,20]. It is worth noting that some implant rejections may result from the disconnection of the implant surface and bone tissue, due to inflammation associated with local infection. To reduce the risk of peri-implant infection, antibiotic prophylaxis is commonly used [21-23]. Nowadays, there is more and more research on the use of materials endowed with local antibacterial activity. Among them, silver-doped coatings (DLC - diamond-like carbon, HAp) seem to be promising [24-28]. As shown in the literature, the introduction of silver into HAp coatings can be carried out in various ways [29,30]. One of the possibilities is the application of powders containing both hydroxyapatite and silver in the coating manufacturing processes [31,32]. The present work addresses precisely this issue. It describes an ion exchange process using hydroxyapatite powder and silver nitrate (V) solutions. The efficiency of such a process is influenced by the following factors: pH, temperature, and the solution concentration where the reaction takes place. pH parameter determines the degree of dissociation of functional groups, which has a bearing on the dynamics and efficiency of the process. On the other hand, increasing the temperature of the process accelerates the ion exchange reaction. This happens due to the internal structure loosening of the ionite particle so that the transport of ions into the structure is much easier. The ion exchange process is also affected by the structure of the ionite particles, the type of ions exchanged, the type and number of functional groups in the ionite, and the efficiency of ionite regeneration [33,34]. The ion exchange processes carried out in this work, using hydroxyapatite powder and different concentrations of silver nitrate (V) solution, enabled the formation of a silver-containing compound (Ag_3PO_4) from which metallic silver can be obtained by annealing [35-37]. Therefore, the paper also includes the results from a trial annealing process of a selected powder at 800°C.

Materials and Methods

Hydroxyapatite ($\text{Ca}_{10}(\text{PO}_4)_6(\text{OH})_2$) powder from MEDICOAT used for the plasma spraying of coatings and the silver nitrate (V) AgNO_3 solution from P.P.H. "STANLAB" Sp. J. were used for the ion exchange process. In the first step, AgNO_3 solutions were prepared at concentrations: 1M and 4M. An appropriately determined mass of silver nitrate AgNO_3 was dissolved in deionized water at 50°C using a magnetic stirrer. An equal amount of hydroxyapatite powder was then added to the solutions. The ion exchange was carried out for a 7 pH solution. To obtain the intended pH of the suspensions, 65% HNO_3 was gradually added. The obtained suspensions were stirred at a constant temperature of 50°C for 30 min. Then, all the suspensions were subjected to decantation three times. Finally, the obtained products were dried for 48 h at room temperature and then for 24 h in a vacuum dryer at 100°C . The obtained samples were designated as Ag-HAp-1M and Ag-HAp-4M, respectively. The sample with the highest concentration of silver was subjected to annealing in a vacuum oven (at about 10^{-3} Pa) at 800°C for 1 hour.

Morphology studies of the modified HAp and Ag-HAp powders were performed using a JSM-6610LV Scanning Electron Microscope (JEOL, USA) equipped with an EDS chemical composition analysis attachment (X-Max 80 EDS; Oxford Instruments, UK). Surface topography images of the samples were taken using secondary electrons. Observations were made under high vacuum, with accelerating voltage from 10 to 15 kV. The phase composition analysis was carried out using an EMPYREAN X-ray diffractometer from PANalytical, operating in Theta-Theta geometry at 40 kV and 45 mA current, using Co lamp X-rays with wavelength $\lambda = 1.7902 \text{ \AA}$. To confirm the changes in the chemical structure of the powders, the Raman Spectroscopy technique was applied, using an inVia Confocal Raman spectrometer from Renishaw (Gloucestershire, UK) using a 532 nm laser.

Results and Discussion

The SEM images show the morphology of the HAp powders before and after the modification processes. FIG. 1a shows the characteristic structure of the HAp powders. As can be seen, there are agglomerates of smaller particles with irregular shapes (FIG. 1a). After the ion exchange processes their morphology changes, which is indicated by more regular particle shapes (FIG. 1b,c). All the samples show a rather large scatter of microparticle sizes from about 20 to $130 \mu\text{m}$. None of the modifications applied significantly changed their sizes.

In order to check the effectiveness of the performed processes, the samples were subjected to the EDS analysis to determine their basic chemical composition (FIG. 2). As can be seen, the Ag-HAp-1M sample had the highest silver content (18.52% on an atomic scale). Usege of the higher concentration of AgNO_3 in the solutions inhibites the ion exchange process, and the powders obtained in this way had about 15.05% silver in their atomic composition.

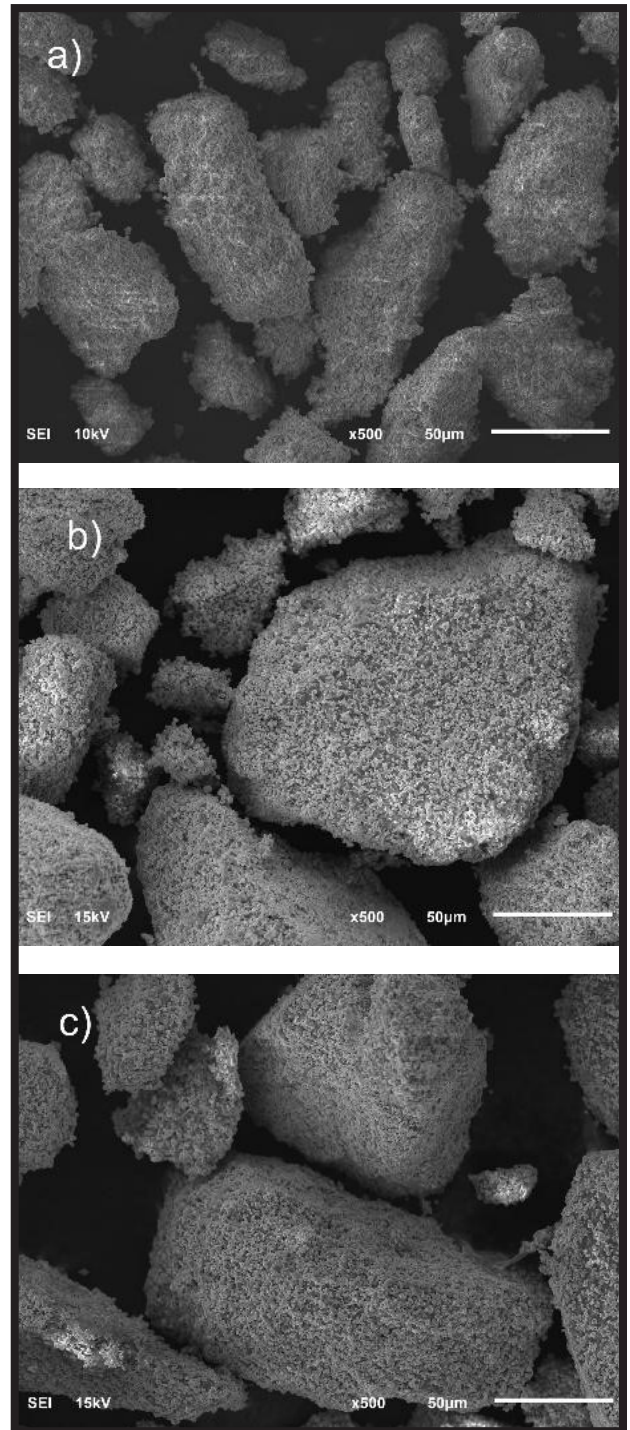


FIG. 1. SEM pictures of surface morphology: a) HAp, b) Ag-HAp-1M, c) Ag-HAp-4M.

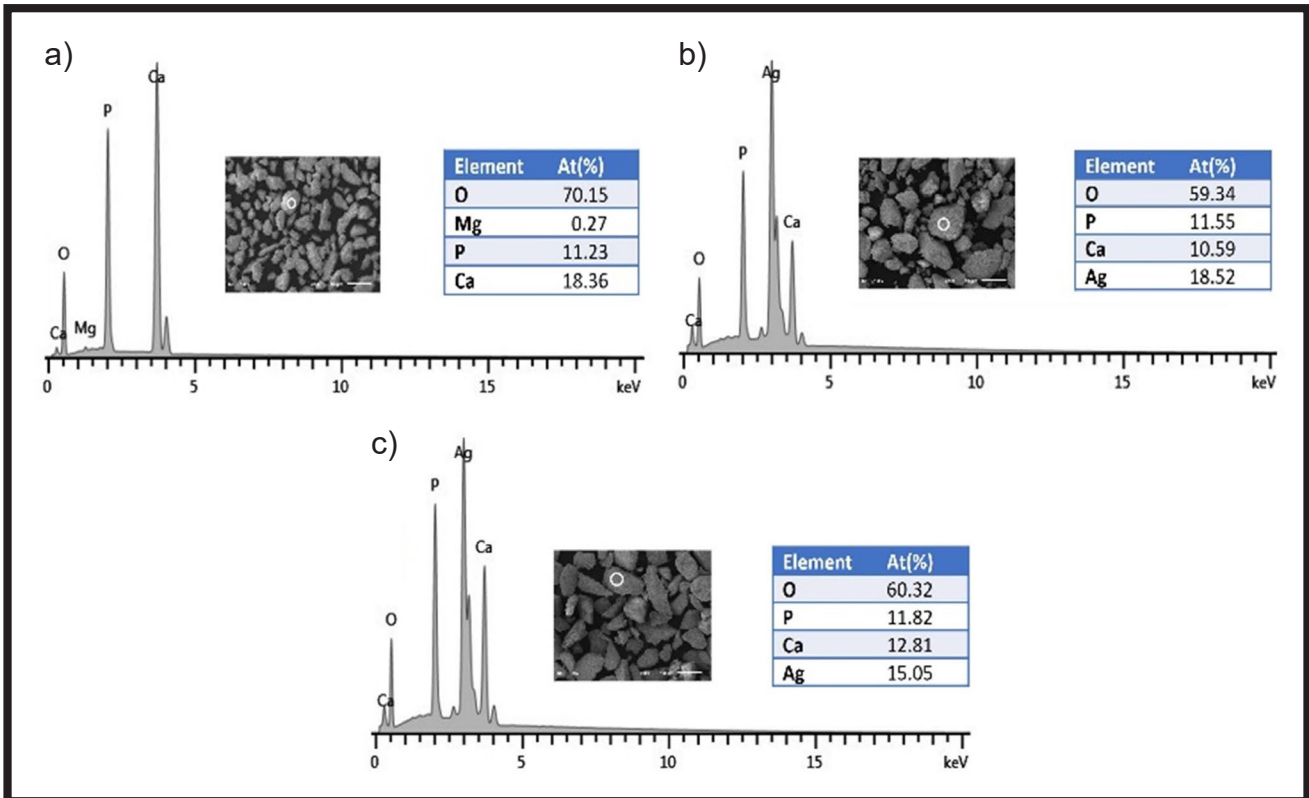


FIG. 2. EDS analysis of the micropowders: a) HAP, b) Ag-HAp-1M, c) Ag-HAp-4M.

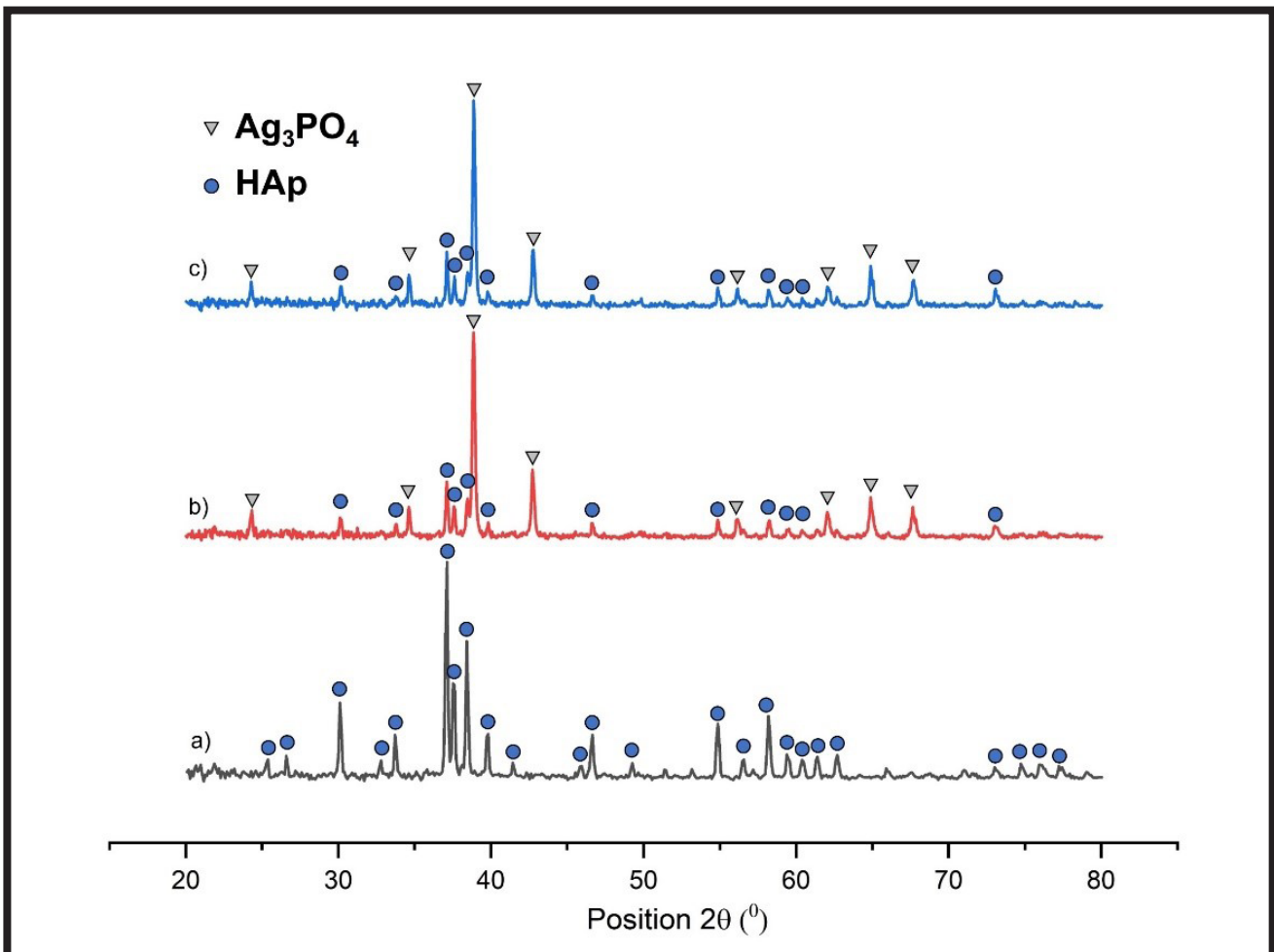


FIG. 3. X-ray patterns of analyzed micropowders: a) HAp, b) Ag-HAp-1M, c) Ag-HAp-4M.

Further analysis of the ion exchange process was made by XRD technique and Raman Spectroscopy. FIG. 3 shows the diffractograms obtained for the powders before and after modification. This study did not reveal any other crystalline phases in the powders except for HAp (according to the standard number 00-009-0432) and Ag_3PO_4 (according to the standard number 04-009-5227). Their simultaneous presence is evidence that the selected conditions enabled only a partial exchange of Ca^{2+} ions to Ag^+ in HAp powders. For HAp powders, distinct diffraction peaks which corresponded to specific crystallographic planes of the hexagonal cell were found at the following angular positions: 25.39 (200); 26.65 (111); 30.14 (002); 32.78 (102); 33.76 (210); 37.07 (211); 37.56 (112); 38.39 (300); 39.75 (202); 41.44 (301); 45.85 (212); 46.58 (310); 49.22 (311); 54.82 (222); 56.49 (312); 58.14 (213); 59.37 (321); 60.33 (410); 61.32 (402); 62.59 (004); 73.04 (214); 74.72 (502); 76.05 (323.304); 77.25 (511). After the modification processes in the powders, in addition to the selected HAp diffraction peaks, the peaks characteristic for the Ag_3PO_4 cubic structure were observed at the following angular positions: 24.30 (110); 34.63 (200); 38.88 (210); 42.76 (211); 56.15 (310); 62.07 (222); 64.91 (320); 67.68 (321). Additionally, the analysis based on the Rietveld method showed that in Ag-HAp-1M powders the Ag_3PO_4 phase accounted for 43.5% while in Ag-HAp-4M powders only 35.2%. The trend of these changes is also visible in the intensity of the characteristic peaks on the diffractograms shown in FIG. 3.

FIG. 4 presents the Raman spectra of the studied powders. The spectrum of the unmodified hydroxyapatite (4a) according to the literature [38-41] shows the most intense peak characteristic of symmetric stretching vibrations around 963 cm^{-1} (character 1) between P-O-P within the $(\text{PO}_4)^{3-}$ tetrahedral.

Further, peaks at about 1072 , 1046 and 1029 cm^{-1} respectively, correspond to the symmetric stretching vibrations. Modes at about 593 and 581 cm^{-1} are associated with (4) O-P-O vibrations and at about 431 cm^{-1} with (2) O-P-O vibrations. After modification in the aqueous AgNO_3 solution, the most prominent peak on the Raman spectrum is at the position of about 909 cm^{-1} originating from the stretching symmetric vibrations of (1) PO_4^{3-} evidently indicating the formation of Ag_3PO_4 [42,43]. In addition, typical modes from the unmodified HAp powder (especially at 963 cm^{-1}) are visible to a lesser extent. For powders modified in AgNO_3 solution, the peaks at 909 cm^{-1} and 963 cm^{-1} change their intensities according to the content of silver atoms in the samples. The lowest intensity of the peak characteristic for the pure HAp powder (at 963 cm^{-1}), and at the same time the highest intensity of the peak characteristic for the Ag_3PO_4 structures (at 909 cm^{-1}) are typical for the Ag-HAp-1M powders with the highest silver content and the highest content of Ag_3PO_4 phase.

The mixture of silver phosphate and hydroxyapatite obtained in the ion exchange process with the highest silver content was subjected to a one-hour annealing process in a vacuum oven at 800°C in order to confirm the possibility of changing the structure of the modified powders to the one with silver in a metallic form and not in the Ag_3PO_4 compound. After this process, the powders were re-examined using the techniques presented earlier. FIG. 5 presents the SEM image of the powder modified in this way along with EDS analysis, while FIG. 6 shows the characteristic XRD and Raman spectroscopy spectra. As can be seen in FIG. 5, the morphology of the powders changed. After the annealing process, the micropowders were composed of spherically shaped, sintered particles.

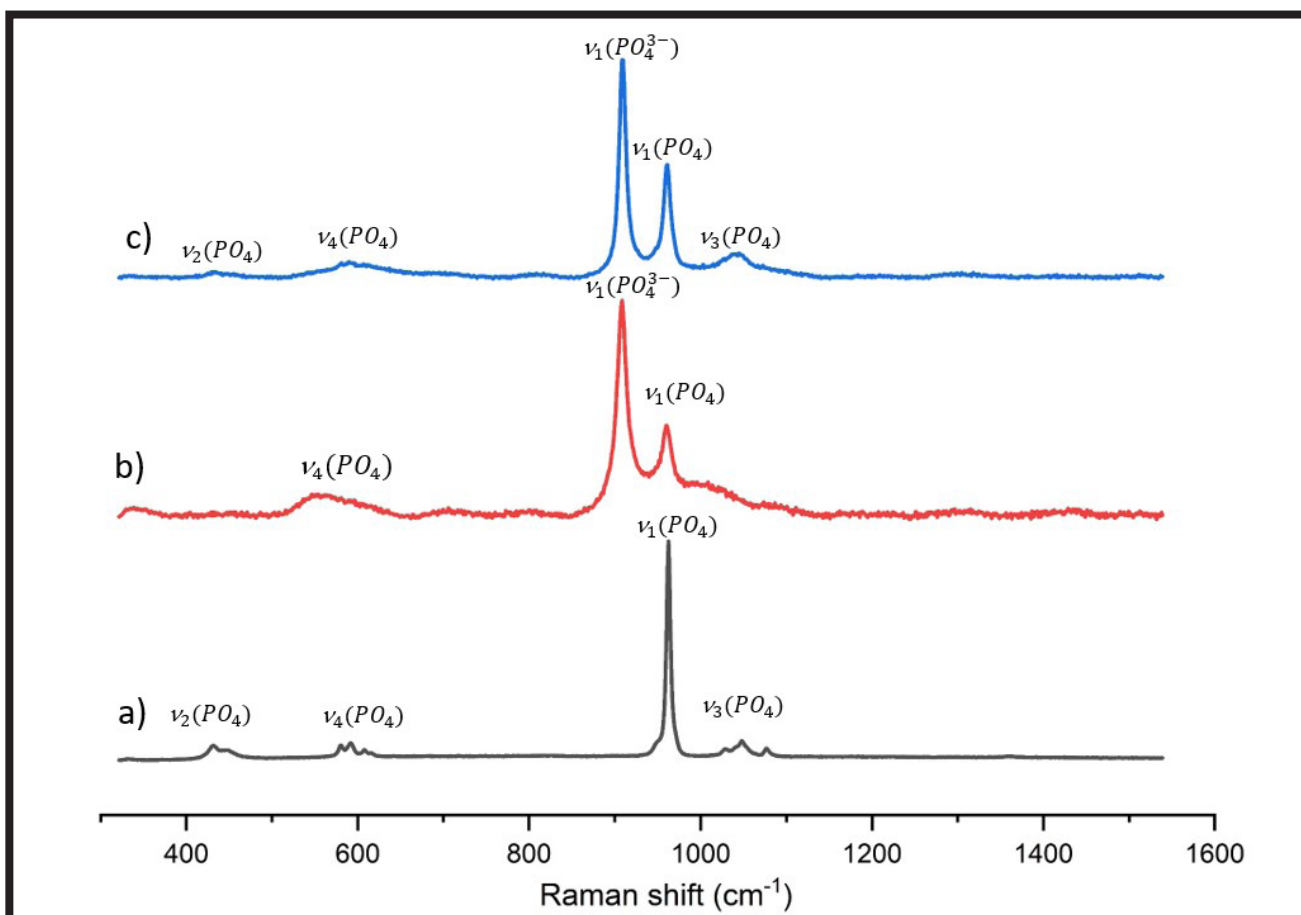


FIG. 4. Raman spectra of micropowders: a) HAp, b) Ag-HAp-1M, c) Ag-HAp-4M.

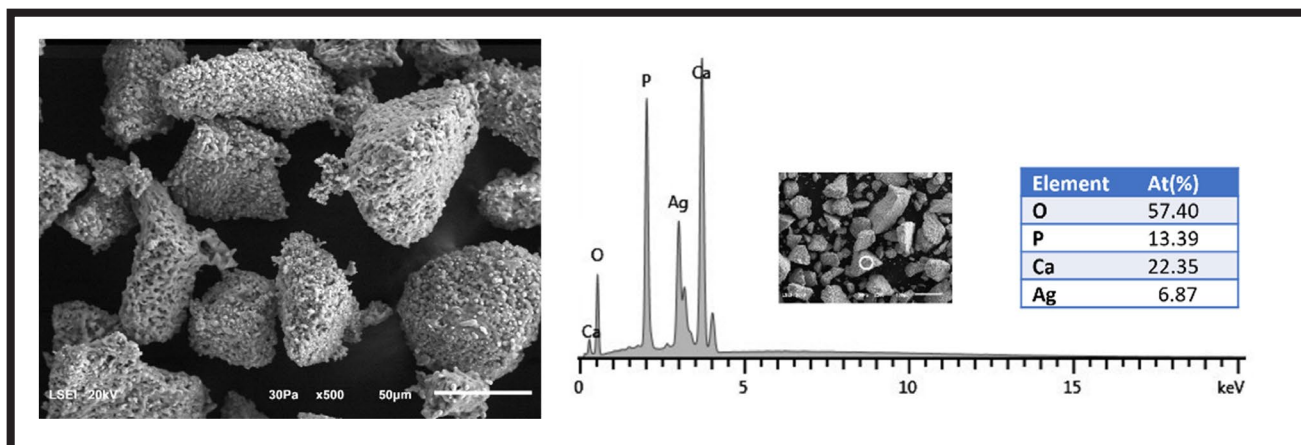


FIG. 5. Surface morphology and EDS analysis of heated micropowders Ag-HAp-1M.

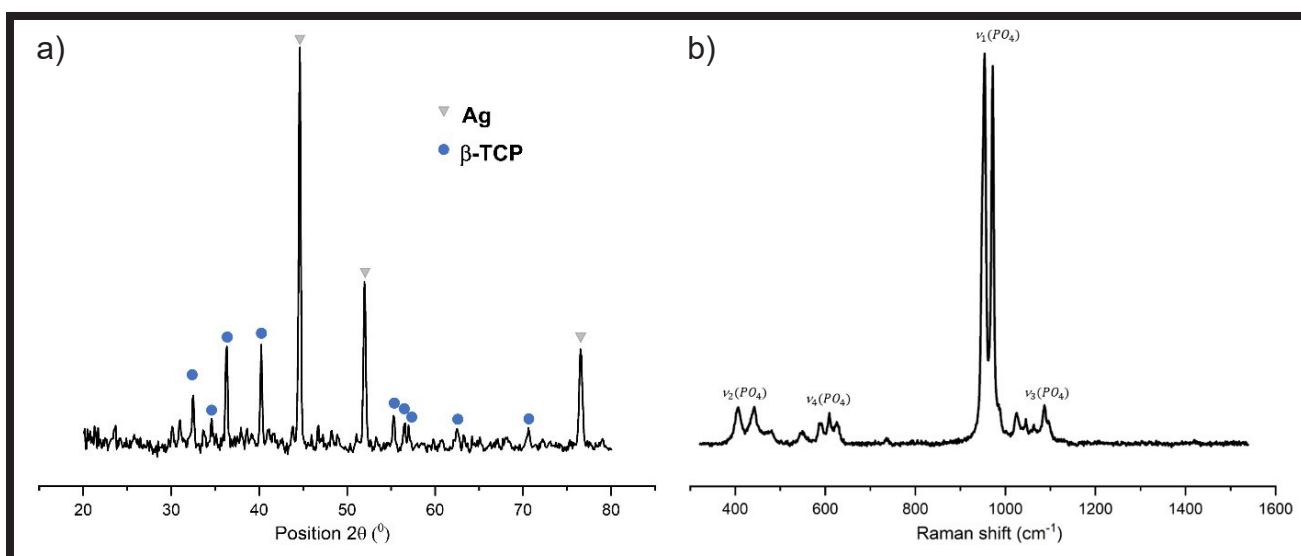


FIG. 6. X-ray pattern of phase composition (a) and Raman spectrum (b) of Ag-HAp-1M powder.

From the EDS studies, it can be seen that the silver content of these powders was lower than the Ag-HAp-1M powders, which may be due to the temperature and pressure of the processing. After annealing, the characteristic peaks of the silver cubic structure were observed in the studied powders (FIG. 6a) at the following angular positions: 44.57 (111); 51.95 (200); 76.53 (220) and rhombohedral -TCP at the following angular positions: 32.36 (214); 34.57 (300); 36.19 (0210); 40.13 (220); 55.13 (4010); 56.33 (238); 56.85 (416); 62.35 (2020); 70.38 (517). The Raman spectrum in FIG. 6b shows the change of the HAp powder in -TCP, as evidenced by the $1(\text{PO}_4)$ modes occurring at about 949 cm^{-1} and 971 cm^{-1} [43-45]. The other peaks were attributed to the $2(\text{PO}_4)$ vibrations occurring at about $406, 442, 481\text{ cm}^{-1}$, $3(\text{PO}_4)$ at about $1016, 1048\text{ cm}^{-1}$, and $4(\text{PO}_4)$ at about $546, 598, 609,$ and 628 cm^{-1} .

Conclusions

The ion exchange process led to the incorporation of silver ions into the hydroxyapatite structure. This confirmed the effectiveness of the procedure used to obtain the powders as $\text{Ag}_3\text{PO}_4/\text{HAp}$ mixtures. The morphology of the HAp powders changes significantly as a result of silver doping. The phase composition analysis revealed the presence of characteristic peaks corresponding to HAp and the newly formed silver phosphate phase Ag_3PO_4 .

The sample modified with 1M AgNO_3 in an aqueous solution had the highest silver content. Additionally, the chemical and phase composition of the produced powders can be modified by thermal treatment. The use of vacuum annealing at 800°C resulted in the formation of metallic silver and the change in the structure of HAp to $\beta\text{-TCP}$. However, further studies and analyses are necessary to precisely develop process parameters for the modification of HAp powders with silver ions, as well as their thermal treatment.

Acknowledgments

Special thanks are directed to the staff of the Institute of Materials Science, Technical University of Lodz, for providing the equipment and creating the possibility to carry out the research part. We would also like to thank MEDGAL Company for providing HAp powders used in this research.

ORCID iDs

M. Gluszek: <https://orcid.org/0000-0002-6096-988X>
 Z. Świrska: <https://orcid.org/0000-0001-8175-2762>
 W. Kaczorowski: <https://orcid.org/0000-0001-7193-0473>
 B. Januszewicz: <https://orcid.org/0000-0001-8735-0975>
 M. Wrotniak: <https://orcid.org/0000-0002-4329-8623>

References

- [1] Ślósarczyk A., Potoczek M., Paszkiewicz Z., Zima A., et al.: Characteristics and biological evaluation of high-porosityapatite bioceramics. *Ceramic Materials* 62(2) (2010) 224-229.
- [2] Sobczak-Kupiec A., Wzorek Z.: Właściwości fizykochemiczne ortofosforanów wapnia istotnych dla medycyny - TCP i HAP. *Chemia. Czasopismo techniczne* 107 (2010) 309-322.
- [3] Kluess D., Bergschmidt P., Mittelmeier, W.: *Ceramics for joint Replacement. Joint Replacement Technology*, (2014) 152-166.
- [4] Gremillard L., Chevalier J.: *New Trends in Ceramics for Orthopedics. Encyclopedia of Materials: Technical Ceramics and Glasses* 3 (2021) 493-500.
- [5] Arcos D., Vallet-Regi M.: Substituted hydroxyapatite coatings of bone implants. *Journal of Materials Chemistry B*, 8(9) (2020) 1781-1800.
- [6] Wang X., Yu Y., Ji L., et al.: Calcium phosphate-based materials regulate osteoclast-mediated osseointegration. *Bioactive Materials* 6(12) (2021) 4517-4530.
- [7] Święcicki Z.: *Bioceramika dla ortopedii. Instytut Podś. Problemy Techniki PAN, Wyd. Spółdzielcze Sp. z o.o., Warsaw, 1992.*
- [8] Rujitanapanich S., Kumpapan P., Wanjanoi P.: Synthesis of Hydroxyapatite from Oyster Shell via Precipitation. *Energy Procedia* 56 (2014) 112-117.
- [9] Szczeń A., Hołysz L., Chibowski E.: Synthesis of hydroxyapatite for biomedical applications, *Advances in Colloid and Interface Science* 249 (2017) 321-330.
- [10] Gaoyu Ch., Xiaoyan Z., Chong W., Junfeng H., et al.: A post-synthetic ion exchange method for tunable doping of hydroxyapatite nanocrystals. *RSC Advances*, 7(89) (2017) 56537-56542.
- [11] Hou J., Liu Y., Han Z., et al.: Silver-hydroxyapatite nanocomposites prepared by three sequential reaction steps in one pot and their bioactivities in vitro. *Materials Science and Engineering C* 120 (2021) 111655.
- [12] Dubnika A., Loca D., Rudovica V., et al.: Functionalized silver doped hydroxyapatite scaffolds for controlled simultaneous silver ion and drug delivery. *Ceramics International* 47 (2017) 3698-3705.
- [13] Šupová M.: Substituted hydroxyapatites for biomedical applications: A review, *Ceramics International* 41(8) (2015) 9203-9231.
- [14] Chen W., Liu Y., Courtney H.S., Betteng M., Agrawal C.M., et al.: In vitro anti-bacterial and biological properties of magnetron co-sputtered silver-containing hydroxyapatite coating. *Biomaterials* 27(32) (2006) 5512-5517.
- [15] Rai M., Yadav A., Gade A., et al.: Silver nanoparticles as a new generation of antimicrobials. *Biotechnology Advances* 27(1) (2009) 76-83.
- [16] Lysakowska M., Denys P.: Antimicrobial uses of silver. *Antimicrobial uses of silver. Ortop 4 Quarter*, (2009) 408-417.
- [17] Klasen H.J.: A historical review of the use of silver in the treatment of burns. II. Renewed interest for silver, *Burns* 26(2) (2000) 131-138.
- [18] Moiem N.S., Shale E., Drysdale K.J., et al.: Acticoat dressings and major burns: Systemic silver absorption. *Burns* 37 (2011) 27-35.
- [19] Bugla-Płoskońska G., Oleszkiewicz A.: Biological activity of silver and its application in medicine. *Cosmos – Problems of Biological Sciences* 56(1-2) (2007) 115-122.
- [20] Yang J.Y., Huang C.Y., Chuang S.S., et al.: Case report: A clinical experience of treating exfoliative wounds using nanocrystalline silver-containing dressings (Acticoat). *Burns* 33 (2007) 793-797.
- [21] Lansdown A.B.G.: Silver. I: its antibacterial properties and mechanism of action. *Journal of Wound Care* 11(4) (2013) 125.
- [22] Petica A., Gavriliu S., Lungua M., et al.: Colloidal silver solutions with antimicrobial properties. *Materials Science and Engineering: B* 152 (2008) 22-27.
- [23] Sandukas S., Yamamoto A., Rabiei A.: Osteoblast adhesion to functionally graded hydroxyapatite coatings doped with silver. *J. Biomed. Mater. Res.* 97(4) (2011) 490-497.
- [24] Ratha I., Datta P., Balla V. K., et al.: Effect of doping in hydroxyapatite as coatings material on biomedical implants by plasma spraying method; A review. *Ceramics International* 47(4) (2021) 4426-4445.
- [25] Ressler A., Žužić A., et al.: Ionic substituted hydroxyapatite for bone regeneration applications: A review. *Open Ceramics* 6 (2021) 100122.
- [26] Lei Song, Yan-Feng, Xiao Lu Gan, et al.: The effect of antibacterial ingredients and coating microstructure on the antibacterial properties of plasma sprayed hydroxyapatite coatings. *Surface and Coatings Technology* 206(11-12) (2012) 2986-2990.
- [27] Kolmas J., Piotrowska U., Kuras M., et al.: Effect of carbonate substitution on physicochemical and biological properties of silver containing hydroxyapatites. *Materials Science and Engineering: C* 74(1) (2017) 124-130.
- [28] Cazalini E.M., Miyakawa W., Teodoro, G.R., et al.: Antimicrobial and anti-biofilm properties of polypropylene meshes coated with metal-containing DLC thin films. *Journal of materials science. Materials in medicine* 28(6) (2017) 97.
- [29] Chen W., Oh S., Ong A.P., Oh N., et al.: Antibacterial and osteogenic properties of silver-containing hydroxyapatite coatings produced using a sol gel process. *The Japanese Society for Biomaterials, and The Australian Society for Biomaterials and the Korean Society for Biomaterials* 82(4) (2007) 899-906.
- [30] Yajing Y., Xuejiao Z., Yong H., et al.: Antibacterial and bioactivity of silver substituted hydroxyapatite/TiO₂ nanotube composite coatings on titanium. *Applied Surface Science* 314(30) (2014) 348-357.
- [31] Bensalema A., Kaan Kucukosman O., Raszkievicz J.: Synthesis, characterization, bactericidal activity, and mechanical properties of hydroxyapatite nano powders impregnated with silver and zinc oxide nanoparticles (Ag-ZnO-Hap). *Ceramics International* 47(15) (2021) 21319-21324.
- [32] Wahhab Abdulsada F., Ali Sabea Hammood: Characterization of corrosion and antibacterial resistance of hydroxyapatite/silver nano particles powder on 2507 duplex stainless steel. *Materialstoday proceedings* 42(5) (2021) 2301-2307.
- [33] Zagorodni A.A.: *Physico-chemical Description of Ion Exchange Processes. Ion Exchange Materials, Properties and Applications*, Elsevier (2007) 169-198.
- [34] De Trizio L., Manna L.: Forging Colloidal Nanostructures via Cation Exchange Reactions. 116(18) (2016) 1085210887.
- [35] M.M.J. van Rijt, S.W. Nooteboom, et al.: Stability-limited ion-exchange of calcium with zinc in biomimetic hydroxyapatite. *Materials & Design* 207 (2021) 109846.
- [36] Riaz M., Zia R., Ijaz A.: Synthesis of monophasic Ag doped hydroxyapatite and evaluation of antibacterial activity. *Materials Science and Engineering: C* 90(1) (2018) 308-313.
- [37] Hong X., Wu X., Zhang Q., Xiao M.: Hydroxyapatite supported Ag₃PO₄ nanoparticles with higher visible light photocatalytic activity. *Applied Surface Science* 258(10) (2012) 4801-4805.
- [38] Chai B., Jing L., Qian X.: Reduced Graphene Oxide Grafted Ag₃PO₄ Composites with Efficient Photocatalytic Activity under Visible-Light Irradiation, *Ind. Eng. Chem. Res.* 53 (2014) 8744-8752.
- [39] Klinkaewnarong J., Swatsitang E., Masingboon Ch., Seraphin S., Maensiri S.: Synthesis and characterization of nanocrystalline HAP powders prepared by using aloe vera plant extracted solution. *Current Applied Physics* 10 (2010) 521-525.
- [40] Silva C.C., Sombra A.S.B.: Raman spectroscopy measurements of hydroxyapatite obtained by mechanical alloying. *Journal of Physics and Chemistry of Solids* 65 (2004) 1031-1033.
- [41] Koutsopoulos S.: Synthesis and characterization of hydroxyapatite crystals: A review study on the analytical methods. *Journal of Biomedical Materials Research* 62 (2002) 600-612.
- [42] Hua T., Yanhui F., Shufang Ch., Siyu X., Guogang T.: Construction of Ag₃PO₄/Ag₂MoO₄ Z-scheme heterogeneous photocatalyst for the remediation of organic pollutants. *Chinese Journal of Catalysis* 38 (2017) 337-347.
- [43] Penel G., Cau E., Delfosse C., Rey Ch., Hardouin P., Jeanfils J., et al.: Raman Microspectrometry Studies of Calcified Tissues and Related Biomaterials. *Raman Studies of Calcium Phosphate Biomaterials. Dent. Med. Probl.* 40(1) (2003) 37-43.
- [44] Carrodegua R.G., De Aza S.: α-Tricalcium phosphate: Synthesis, properties and biomedical applications. *Acta Biomaterialia* 7 (2011) 3536-3546.
- [45] Aruna S.T., Kulkarni S., Chakraborty M., et al.: A comparative study on the synthesis and properties of suspension and solution precursor plasma sprayed hydroxyapatite coatings. *Ceramics International* 43 (2017) 9715-9722.

THE ENCAPSULATION OF ANTIBACTERIAL DRUGS IN POLYMER NANOPARTICLES AND THEIR USE IN DRUG DELIVERY SYSTEMS ON ZrO₂ SCAFFOLD WITH BIOACTIVE COATING

IWONA PUDELKO^{1*}, GAËLLE DESANTE²,
ELŻBIETA PAMUŁA¹, KAROLINA SCHICKLE²,
MAŁGORZATA KROK-BORKOWICZ¹

¹ AGH UNIVERSITY OF SCIENCE AND TECHNOLOGY,
FACULTY OF MATERIALS SCIENCE AND CERAMICS,
AL. MICKIEWICZA 30, 30-059 KRAKÓW, POLAND

² RWTH AACHEN UNIVERSITY,
DEPARTMENT OF CERAMICS AND REFRACTORY MATERIALS,
MAUERSTRASSE 5, 52064 AACHEN,
NORTH RHINE-WESTPHALIA, GERMANY

*E-MAIL: IPUDELKO@AGH.EDU.PL

Abstract

Bone infections are a challenging problem as they may cause a permanent patient disability and even death. Additionally, their relapse rate is relatively high. The implantation of a local drug delivery system can be an effective way to fight bone infections. In this study, we present the process of surface bioactivation and immobilization of nanoparticles loaded with drugs. Our aim was to improve osseointegration of the ZrO₂ surface by coating it with a bioactive layer containing poly(L-lactide-co-glycolide) (PLGA) nanoparticles (NPs) loaded with antibacterial drugs (gentamicin and bacitracin) using a biomimetic precipitation method. The ZrO₂ substrates were prepared via pressing and sintering. The CaP-coating was obtained by immersing the substrates in ten-times concentrated simulated body fluid (10×SBF). NPs were prepared by the double emulsion method and the drug loading in NPs was assessed. Thus obtained NPs were applied on bioactivated ceramic substrates by the drop-casting method or by introducing them in the 10×SBF solution during the bioactivation process. The NPs were visualized using scanning electron microscopy (SEM). The NPs size and the Zeta potential were measured using dynamic light scattering (DLS) method. The microstructure of the coating and the efficiency of the NPs incorporation were tested by SEM. In this study, we proved the presented process to be an effective way to obtain biomaterials that could be used as drug delivery systems to treat bone infections in the future.

Keywords: bioactivation, polymer nanoparticles, bioactive layer, biomimetic coating, bone tissue regeneration, bone implants

[Engineering of Biomaterials 161 (2021) 21-27]

doi:10.34821/eng.biomat.161.2021.21-27



Copyright © 2021 by the authors. Some rights reserved.
Except otherwise noted, this work is licensed under
<https://creativecommons.org/licenses/by/4.0>

Introduction

Nowadays, bone infections are a widespread problem. Due to the limited ability of the antibiotics accumulation in the bone tissue, the infection treatment is rather difficult [1]. The increasing average age of the patients contributes to the reduction of immune response, more hip fractures and higher numbers of joint surgeries. The increasing number of joint infections is also a result of the overall population aging [2,3]. Bone infections are often extremely painful and lead to progressive destruction, abnormal bone formation and the body's systemic inflammatory response. As a consequence, they may cause permanent disability and even death [4,5]. Despite the availability of a large number of antibiotics, bone infections remain a challenge for clinicians and have a high relapse rate despite the seemingly effective treatment [6].

Bone and marrow infections can be caused by any pyogenic organism, as well as by some strains of fungi, but the most common pathogens are Gram-positive bacteria, including *Staphylococcus aureus* that causes 80% of osteomyelitis. Gentamicin sulfate is the most commonly used antibiotic to impair the bacterial protein synthesis and thus to prevent the infection from spreading [3,4].

S. aureus releases bacterial adhesins that help it stick to the host extracellular matrix proteins, which is the first step in the infection pathogenesis. Additionally, *S. aureus* shows the ability to effectively evade the human immune system, to penetrate mammalian cells and to persist intracellularly, which is one of the main reasons for the high recurrence rate of osteomyelitis [4,7].

The treatment of bone infections is based on a long-term and aggressive antibiotic therapy which is the last and the longest stage of the treatment and may last up to several weeks. The choice of active substance and the therapy duration depends on the patient risk factors, comorbidities or the presence of drug-resistant microorganisms. The chronic osteomyelitis treatment generally involves several steps. The first is to clean up the necrotic and infected tissue. Then, the defective area needs to be filled in to start the bone repair or regeneration process. Only then the antibiotics are administered [4,8,9].

Antibiotics can be delivered in a variety of ways. The oral drug administration is very rare due to the low concentration of active substances that can reach the bones. That is why, intravenous antibiotics are commonly used, but such a therapy is not always effective and the disease recurs. The unsuccessful intravenous antibiotic delivery results from the fact that the infected bone fragment is often surrounded by sclerotic avascular bone, making it almost inaccessible to systemic antibiotics. For this reason, it is often necessary to remove the infected bone. The solution to this problem may be the implantation of a drug delivery system with an extended release time in order to ensure the appropriate concentration of antibiotics for a longer period of time. In general, the local drug delivery is regarded as more effective in fighting the disease than the systemic therapy [8,9].

Gentamicin, or rather gentamicin sulfate, is an aminoglycoside antibiotic that acts as an inhibitor of the protein synthesis process, binding the 30S subunit of the bacterial ribosome, thus preventing the appearance and spreading of infection. This antibiotic can be used when the use of potentially less toxic drugs is contraindicated. Gentamicin should be used in the treatment of infections caused by susceptible bacteria [3].

Bacitracin is a polypeptide antibiotic that is produced by bacterial strains of *Bacillus subtilis* and *Bacillus licheniformis*. It has an antibacterial effect against Gram-positive bacteria, and also inhibits the resistance to *S. aureus*. The most common side effect of the use of bacitracin is the renal dysfunction but it does not cause complications in the topical application. This side effect is sometimes observed after intravenous systemic administration, while bacitracin taken orally, is safe. In addition, it has been shown that bacitracin can support the osteogenic differentiation of bone marrow stem cells (hBMSC). The high bioactivity of bacitracin as well as its multifunctional properties make this antibiotic effective for the local treatment of bone infections and osteolysis [10-12].

Drug delivery systems (DDS) are considered an extremely valuable tool in modern medicine. They maintain the proper drug concentration in target tissues for a specified period of time, while preventing structural changes of the active substances. These systems are most often based on various types of drug carriers, in particular nanoparticles. The NPs use has a number of advantages. NPs are characterized by a high ability to encapsulate the drug. Their small size allows them to be administered in various ways: orally, intravenously, and even by inhalation. They can reach even the smallest capillaries. In addition, nanoparticles have the ability to penetrate the bone structure, which allows them to reach the infected bone areas [13,14].

In the treatment of bone infections supported by the implant, DDS systems based on biodegradable material can be successfully used. The use of poly(L-lactide-co-glycolide) (PLGA) nanoparticles as a layer allows the design of unconventional scaffolds that provide better functionality. Such an implant, in addition to its basic function, can also play the role of a local delivery system not only for drugs, but also for growth factors or other molecules accelerating the bone tissue regeneration [15].

Zirconium oxide is a material classified as non-bioactive bioceramics. It is characterized not only by high biocompatibility but also by good tribological properties, high strength, and hardness [16,17]. Hydroxyapatite (HAp) is a biocompatible bioceramic material with the molecular formula $\text{Ca}_{10}(\text{PO}_4)_6(\text{OH})_2$, used in bone tissue engineering. This material is bioactive and has osteoconductive properties [16,18].

Bioinert materials can be coated with bioactive layers so as to improve their osseointegration. For this purpose, biocompatible materials are used which should also be osteoconductive and/or osteoinductive, as well as mechanically stable under physiological stress. They should also adhere to the implant. The coating materials are mainly calcium phosphates [16]. The presence of the ceramic bioactive coating increases the implant surface activity by promoting the adhesion and proliferation of osteoblasts and osteogenic cells, which accelerates the process of tissue repair and new bone formation [19,20].

The aim of this study was to bioactivate the bioinert surface of ZrO_2 substrate by coating it with a bioactive layer of calcium phosphate (CaP) that was doped with PLGA NPs loaded with antibacterial drugs using the biomimetic co-deposition method.

Materials and Methods

Preparation of ceramic substrates

The ceramic substrates were obtained via pressing and sintering. Briefly, 1.3 g of the ZrO_2 powder (TZ-3YS-E, Tosoh Corporation, Nanyo Manufacturing Complex, Japan) was uniaxially pressed with a force of 15 kN for 1 min and then sintered for 2 h at the temperature of 1450°C. The produced samples (2 mm thick round lozenges of 1 cm in diameter) were grinded and polished with SiC abrasive papers until the 15 μm grit. Then they were cleaned 4 times by using ultrasounds: twice with acetone (CH_3COCH_3 , Merck KGaA, Darmstadt, Germany), once with ethanol ($\text{C}_2\text{H}_5\text{OH}$, Merck KGaA, Darmstadt, Germany) and once with double distilled water. Having been cleaned, the substrates were immersed in the 5 M phosphoric acid for 3 days at 37°C.

Preparation of nanoparticles

The method of double emulsion with solvent evaporation was used to prepare the nanoparticles. A 2% solution of PLGA (La:Ga ratio 85:15, Mn = 100 kDa, d = 1.5, produced at the Center of Polymer and Carbon Materials, Polish Academy of Sciences, Zabrze, Poland) in dichloromethane (DCM, Avantor Performance Materials, Gliwice, Poland) and a 2% aqueous solution of polyvinyl alcohol (PVA, Sigma Aldrich, Germany) were prepared. Gentamicin (Gent, Sigma Aldrich, Germany) or bacitracin (Bct, Sigma Aldrich, Germany) respectively, in the amount of 6 mg, were added to 3 ml of the PLGA solution, and then homogenized with ultrasound for 3 min with an amplitude of 40% (Sonics, Vibra Cell VCX130, Newtown, CT, USA). The obtained emulsion was added to 20 ml of the PVA solution and stirred at 1000 rpm for 24 h at room temperature. In the next stage, the obtained nanoparticles were centrifuged five times (18000 rpm, 20 min, 4°C), and subsequently they were frozen at -80°C. The last step was the drying process that was carried out in the freeze-dryer (Christ Alpha 1-2 LDplus, Germany) for 24 h.

The morphology of obtained NPs was observed with scanning electron microscope (SEM, GeminiSEM 500, Zeiss, Jena, Germany). Their size and the Zeta potential were measured by dynamic light scattering method (DLS, Zetasizer nano-ZS, Malvern, UK). The encapsulation efficiency was checked by the fluorescence reader (FLUOstar Omega, BMG Labtech, Germany). We used the reaction with o-phthalaldehyde (OPA) and the phenomenon of fluorescence to quantify drugs.

Bioactivation process

We used the biomimetic precipitation method to bioactivate the ZrO_2 surface. In general, the ceramic substrates were immersed in a 10×SBF solution to obtain a bioactive layer. The process was carried out in two stages and it was a combination of two different techniques already described. The first step was based on the paper of A. Tas *et al.*, while the second one on the study of D. Costa *et al.* [21,22]. TABLE 1 shows the reagents and their quantities that were used to prepare the SBF-solutions.

TABLE 1. Reagents used to prepare 1 L of SBF-solution for each step.

Reagent	First step (1000 ml)		Second step (1000 ml)	
	Ca-solution (500 ml)	P-solution (500 ml)	Ca-solution (500 ml)	P-solution (500 ml)
	Mass [g]		Mass [g]	
NaCl	29.220	29.220	41.492	41.492
KCl	0.373	-	-	-
$\text{CaCl}_2 \cdot 2\text{H}_2\text{O}$	3.675	-	3.676	-
$\text{MgCl}_2 \cdot 6\text{H}_2\text{O}$	1.017	-	-	-
$\text{NaH}_2\text{PO}_4 \cdot 2\text{H}_2\text{O}$	-	1.560	-	-
NaHCO_3	-	0.840	-	-
K_2HPO_4	-	-	-	1.742

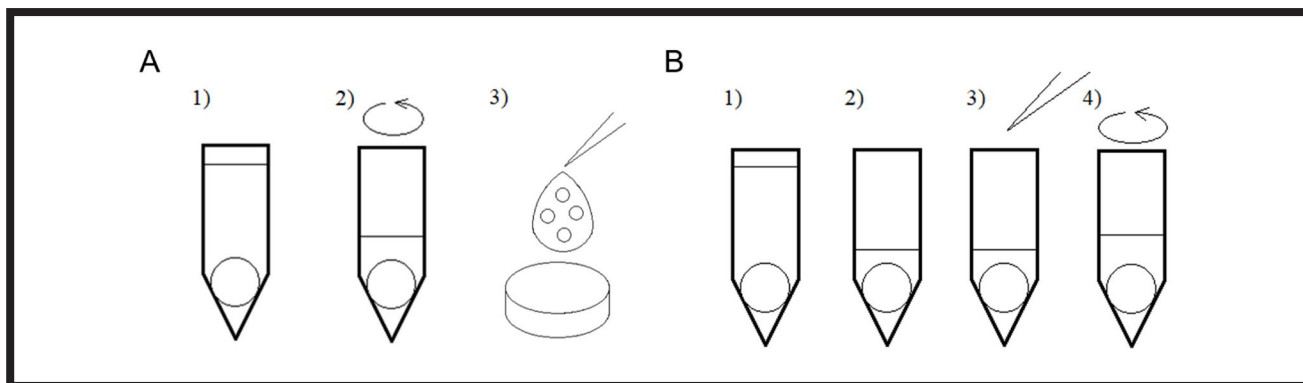


FIG. 1. Schematic representation of the drop casting method (A: 1 – first step of coating process (15 ml of the SBF-solution); 2 – second step of coating process (2.5 ml of the SBF-solution); 3 – adding a drop of dispersed NPs on the coated sample) and the precipitation process (B: 1 – first step of coating process (15 ml of solution); 2 – adding SBF-solution used in the second step; 3 – adding dispersed NPs; 4 – second step of coating process).

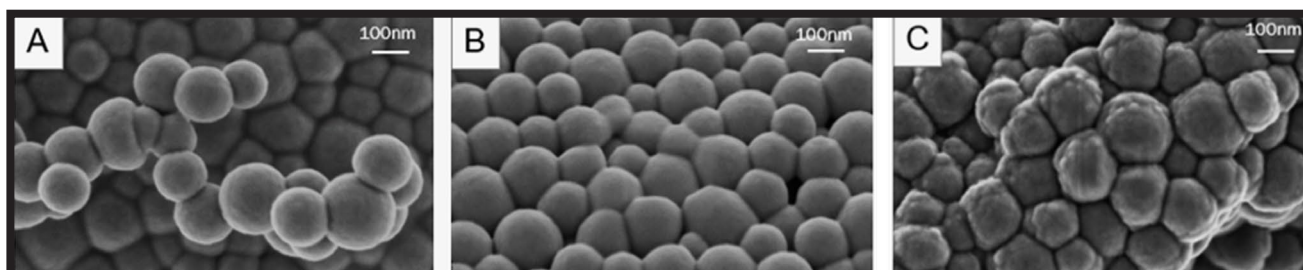


FIG. 2. SEM images of different types of nanoparticles: A – empty nanoparticles (PLGA); B – nanoparticles loaded with gentamicin (PLGA_Gent); C – nanoparticles loaded with bacitracin (PLGA_Bct).

In the first step, the samples were incubated in 15 ml of the SBF-solution for 24 h at 37°C under static conditions. During the second step, they were immersed in 2.5 ml of the SBF-solution for the same period of time but under dynamic conditions (shaking at a speed of 150 rpm) at room temperature. Then, the samples were rinsed three times with double distilled water (ddH₂O) and left to dry.

The microstructure and the quality of received coatings were observed using SEM.

Introducing NPs into the CaP-coating

To introduce NPs onto the ceramic substrates, we used two different methods whose schematic representations are shown in FIG. 1. The first one was the drop-casting method which is based on placing a drop of the NPs dispersed in water on the coated substrate. We applied 100 μ l of dispersion with a NPs-concentration of 2 mg/ml. Then, the samples were dried at room temperature for 48 h. The second method included NPs in the SBF solution during the second step of the bioactivation process. We added 5 mg of NPs to 2.5 ml of the SBF solution to receive the same concentration (2 mg/ml) as in the first method.

To check the efficiency of the immobilization of NPs we analyzed the surface of substrates with SEM.

Results and Discussion

The results of the SEM observation of NPs are presented in FIG. 2. Picture A shows empty NPs while in the pictures B and C there are NPs loaded with gentamicin and bacitracin, respectively. The particles are agglomerated, yet their size is similar in every case, despite the NPs type. NPs are round and regular in pictures A and B, while bacitracin has an impact on the shape and morphology of NPs and makes them more irregular.

DLS results confirmed that the NPs size is similar in every case - approximately 200 nm. However, the size (FIG. 3) as well as the Zeta potential (FIG. 4) are dependent on the NPs type. As shown in TABLE 2, particles loaded with drugs are smaller (207.4 nm and 202.4 nm for particles loaded with gentamicin and bacitracin, respectively) and their Zeta potential increases (-23.9 mV for gentamicin and -13.4 mV for bacitracin) in comparison with the empty NPs whose size and Zeta potential are equal to 226.3 nm and -30.5 mV, respectively. This phenomenon results from the interaction of polymer with drugs whose positive nature changes the polymer surface charge. The encapsulation efficiency is higher for gentamicin (54.3%) in comparison with bacitracin (37.5%) but it is relatively high for both used drugs.

Coating the implant with a bioactive layer is a relatively common method to improve osseointegration. Different methods of the CaP-precipitation on the implant surface have been developed. A. Tas *et al.* created a layer of calcium phosphate on the surface of Ti6Al4V [21]. SBF with a ten times higher concentration (10 \times SBF) of calcium and phosphate ions was used. That solution did not require the use of buffering agents and the coating process itself was carried out at a linear speed. Before dipping in the 10 \times SBF, the Ti6Al4V surface was initially chemically etched in a 5 M KOH solution and then thermally treated at 600°C. The SBF solution made it possible to obtain a calcium phosphate coating not only on metals but also on ceramics or polymers. This method led to the formation of layers in as little as 2 - 6 hours at room temperature. The phosphate content in the coating and the Ca/P molar ratio made the coating classified as bone-like, which is additionally characterized by a relatively high adhesive force to the substrate surface.

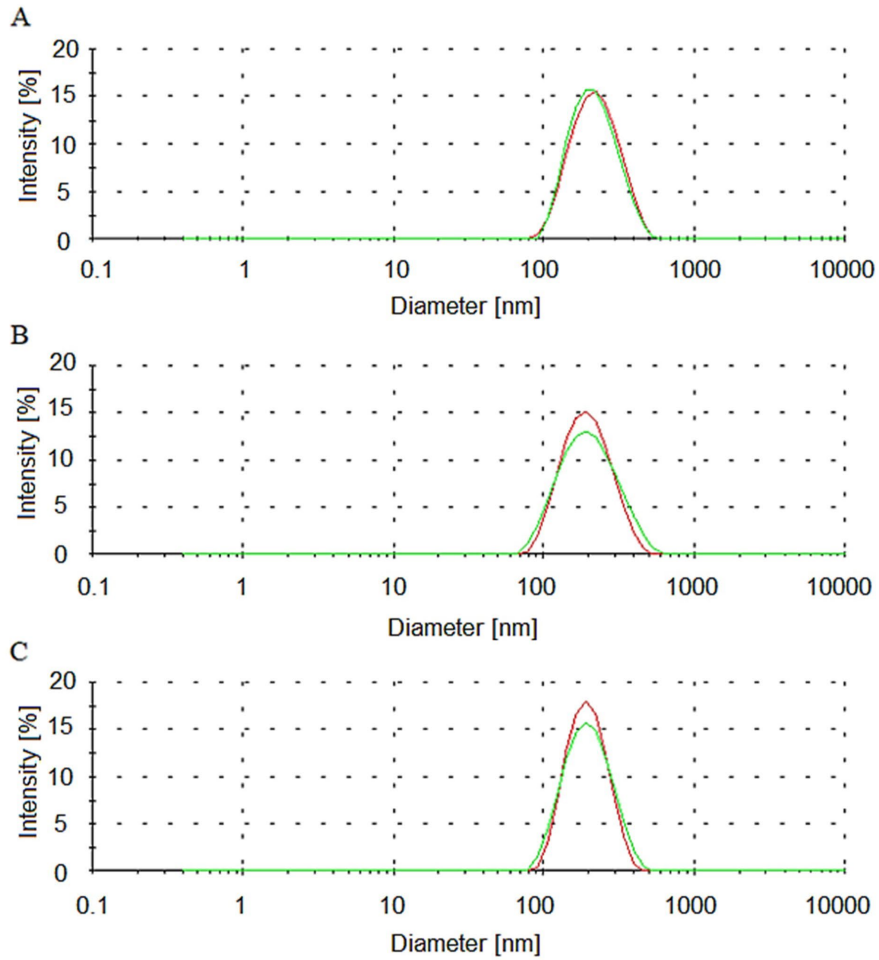


FIG. 3. Size distribution of nanoparticles determined by DLS method: A – PLGA, B – PLGA_Gent, C – PLGA_Bct.

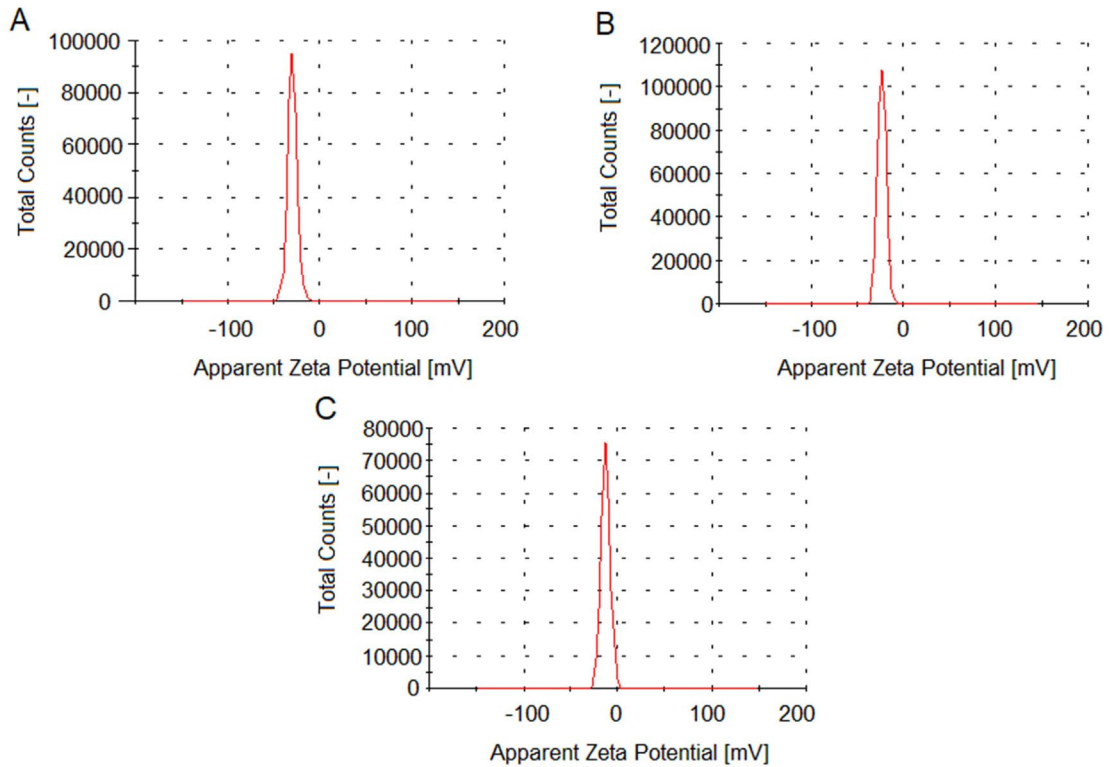


FIG. 4. Zeta potential distribution of nanoparticles: A – PLGA, B – PLGA_Gent, C – PLGA_Bct.

TABLE 2. Characteristics of NPs: average size, Zeta potential and encapsulation of drugs.

	Average size [nm]	Zeta potential [mV]	Encapsulation [%]
PLGA	226.3	-30.5	-
PLGA_Gent	207.4	-23.9	54.3
PLGA_Bct	202.4	-13.4	37.5

D. Costa *et al.* used simulated body fluid (SBF) to create a calcium phosphate (CaP) coating on polycaprolactone (PCL) foil [22]. Due to the presence of such a coating, the polymer substrates could be bioactive and osteoconductive, and their biocompatibility increased when compared to uncoated substrates. The hydroxyapatite (HAp) layer was obtained by dipping the substrate in SBF solution with a five times higher ion concentration (5×SBF) of the typical SBF solution, therefore the time needed to obtain the coating shortened from about 7 days to 24 hours. The coating process was based on the work of Tas *et al.* [21]. The bone-like layers with different surface topography were produced on the PCL substrates, depending on the concentration of Mg^{2+} and HCO_3^- ions. The lower concentrations resulted in a fine surface topography, while high concentrations in a surface with roughness considered optimal for adherence and differentiation of osteoblasts. At the same time, the mechanical properties of CaP coatings were similar to those of natural bone tissue.

In our study, we combined both of the above-mentioned approaches. One method is based on the composition of the blood plasma while the other one contains only the most typical SBF ions. The absence of ions such as Mg^{2+} in the second step transforms the structure obtained in the first step into the more bone-like structure. The first step of our bioactivation process was based on the work of A. Tas *et al.*, while the second one was inspired by the research of D. Costa *et al.* [21,22].

In each stage, we used the Ca- and P-solutions that contained only appropriate ions. When adding the solutions to the tube we followed the order: first P- and then Ca-solution. We immersed the substrates for 24 h at 37°C under static conditions in 15 ml of the solution (7.5 ml of the P- and 7.5 ml of Ca-solution) prepared as shown in TABLE 1. During the second stage, the samples were incubated for the same period of time at room temperature under dynamic conditions (shaking at a speed of 150 rpm), in 2.5 ml of the 10×SBF solution (1.25 ml of the P- and 1.25 ml of Ca-solution) that was prepared as presented in TABLE 1. Then, the samples were rinsed three times with double distilled water (ddH₂O) and left to dry.

The bioactive layers we received correlated with those obtained in the above-mentioned papers, as presented in the SEM pictures A and B (FIG. 5).

Crystals obtained according to the first step of coating process (FIG. 5A) were thinner, while those after both steps (first and second) were thicker and the layer was denser (FIG. 5B).

In order to immobilize NPs on ceramic substrates we used two different methods. One of them was the drop-casting method (FIG. 5C). The other was based on the presence of NPs in the SBF solution during the second step of co-deposition process (FIG. 5D). In both methods the same concentration of dispersed NPs (2 mg/ml) was applied.

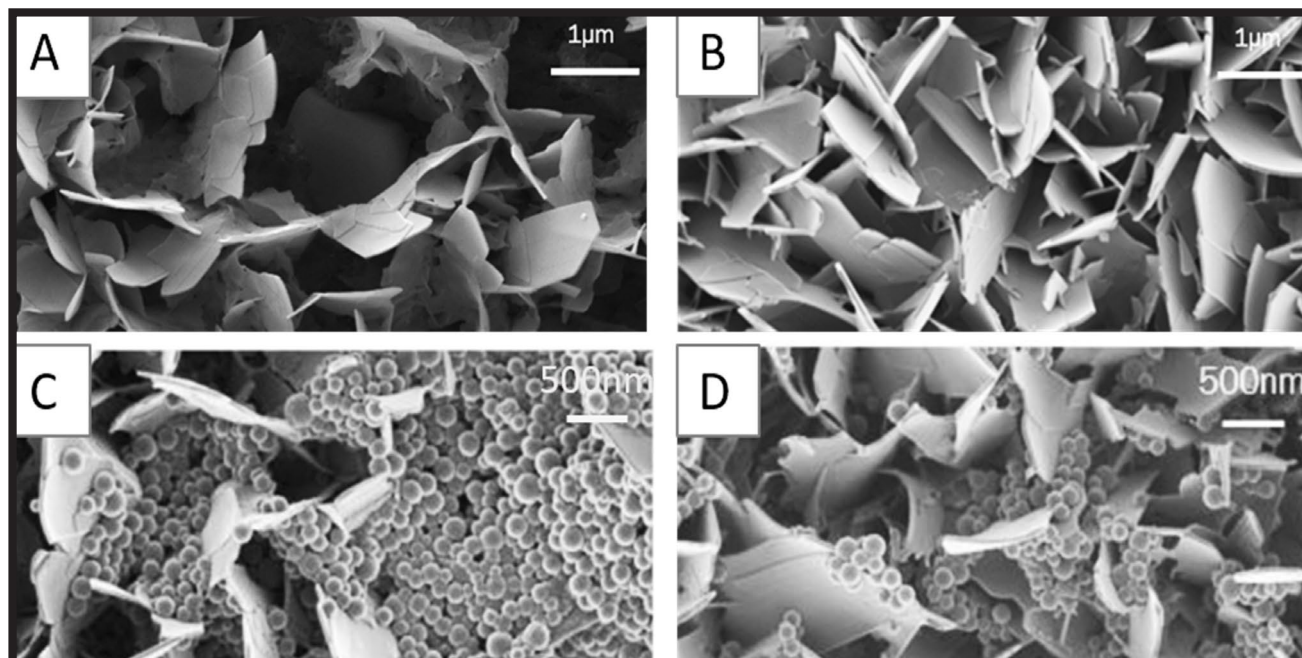


FIG. 5. SEM microphotographs of the bioactive layer on the ZrO_2 substrate after the first (A) and the second (B) step of the coating process and NPs deposited on the ZrO_2 substrates by drop-sitting method (C) and during the CaP layer preparation process (D).

As for the immobilization during co-deposition, the microstructure of bioactive layer did not differ from the one obtained without particles. That means that the NPs presence in the solution did not have a negative impact on the crystallization process. The NPs were evenly distributed on the surface and their adhesion to the surface was relatively strong.

Thanks to the drop-casting method, a larger number of NPs was immobilized so they nearly covered the whole surface. Although they were highly agglomerated and not homogeneously distributed, the NPs deposition was more precise in this method and the adhesion to the bioactive layer was also high.

Conclusions

In this paper we presented a method of producing ZrO_2 substrates coated with a bioactive layer containing polymer nanoparticles loaded with antibacterial drugs.

The biomimetic method of the bioactive layer deposition was stable and the obtained coatings consisted of flake-like crystals. In the first step of the process, the crystals were not fully developed. Therefore, it was important to perform the second step. During that stage, the microstructure transformed into a more stable form which was similar to hydroxyapatite. That explains the necessity of using the two-step process.

Both methods of the NPs immobilization were efficient. However, the number of deposited particles was higher in the drop-casting method. The NPs formed a layer that covered the surface almost completely. In both cases, NPs were agglomerated. Incorporating NPs in the solution during the coating process allowed for a more homogenous particles distribution on the surface of the ZrO_2 substrate. Yet, the immobilization process during co-deposition was less precise because the attached NPs could not be controlled in terms of their quantity.

It can be stated that the method used to prepare nanoparticles was characterized by high stability and efficiency and the obtained particles were of a spherical shape and a desirable size. The presented process of deposition of bioactive layers was an effective technique to bioactivate bioinert surfaces, the result of which was the layer consisting of flake-like crystals. Both methods of immobilizing nanoparticles allowed for the deposition of a sufficient number of particles that were relatively well attached to the substrate. The presented processes of the surface bioactivation and the NPs immobilization are a successful method of creating bioactive ceramic substrates. In further studies we are planning to test the drug release, antibacterial properties and biological properties of our biomaterials in contact with bone cells so as to confirm their potential for tissue engineering and the bone infections treatment.

Acknowledgements

This study was funded by the National Science Center, Poland (2016/21/D/ST8/01685) and by the Program "Excellence Initiative – Research University" for the AGH University of Science and Technology.

ORCID iDs

I. Pudelko:  <https://orcid.org/0000-0002-1024-9374>
 G. Desante:  <https://orcid.org/0000-0001-6340-5126>
 E. Pamuła:  <https://orcid.org/0000-0002-0464-6189>
 K. Schickle:  <https://orcid.org/0000-0003-0944-6917>
 M. Krok-Borkowicz:  <https://orcid.org/0000-0002-9415-0282>

References

- [1] S.G. Rotman, K. Thompson, D.W. Grijpma, R.G. Richards, T.F. Moriarty, D. Eglin, O. Guillaume: Development of bone seeker-functionalised microspheres as a targeted local antibiotic delivery system for bone infections. *Journal of Orthopaedic Translation* 21 (2020) 136-145.
- [2] R. Nair, M.L. Schweizer, N. Singh: Septic Arthritis and Prosthetic Joint Infections in Older Adults. *Infectious Disease Clinics of North America* 31(4) (2017) 715-729.
- [3] U. Posadowska, M. Brzychczy-Wloch, E. Pamuła: Gentamicin loaded PLGA nanoparticles as local drug delivery system for the osteomyelitis treatment. *Acta of Bioengineering and Biomechanics* 17(3) (2015) 41-47.
- [4] K.D. Alder, I. Lee, A.M. Munger, H.-K. Kwon, M.T. Morris, S.V. Cahill, J. Back, K.E. Yu, F.Y. Lee: Intracellular Staphylococcus aureus in bone and joint infections: A mechanism of disease recurrence, inflammation, and bone and cartilage destruction. *Bone* 141 (2020) 115568.
- [5] R.H. Tang, J. Yang, J. Fei: New perspectives on traumatic bone infections. *Chinese Journal of Traumatology - English Edition* 23(6) (2020) 314-318.
- [6] B. Spellberg, B.A. Lipsky: Systemic antibiotic therapy for chronic osteomyelitis in adults. *Clinical Infectious Diseases* 54(3) (2012) 393-407.
- [7] S.K. Nandi, S. Bandyopadhyay, P. Das, I. Samanta, P. Mukherjee, S. Roy, B. Kundu: Understanding osteomyelitis and its treatment through local drug delivery system. *Biotechnology Advances* 34(8) (2016) 1305-1317.
- [8] S. Gitelis, G.T. Brebach: The treatment of chronic osteomyelitis with a biodegradable antibiotic-impregnated implant. *Journal of Orthopaedic Surgery* 10(1) (2002) 53-60.
- [9] D. Neut, O.S. Kluin, B.J. Crielaard, H.C. Van Der Mei, H.J. Busscher, D.W. Grijpma: A biodegradable antibiotic delivery system based on poly-(trimethylene carbonate) for the treatment of osteomyelitis. *Acta Orthopaedica* 80(5) (2009) 514-519.
- [10] B. Nie, H. Ao, J. Zhou, T. Tang, B. Yue: Biofunctionalization of titanium with bacitracin immobilizations shows potential for anti-bacteria, osteogenesis and reduction of macrophage inflammation. *Colloids Surfaces B: Biointerfaces* 145 (2016) 728-739.
- [11] H. Li, B. Nie, Z. Du, S. Zhang, T. Long, B. Yue: Bacitracin promotes osteogenic differentiation of human bone marrow mesenchymal stem cells by stimulating the bone morphogenetic protein-2/Smad axis. *Biomedicine and Pharmacotherapy* 103 (2018) 588-597.
- [12] L.J. Ming, J.D. Epperson: Metal binding and structure-activity relationship of the metalloantibiotic peptide bacitracin. *Journal of Inorganic Biochemistry* 91(1) (2002) 46-58.
- [13] T. Jiang, X. Yu, E.J. Carbone, C. Nelson, H.M. Kan, K.W.H. Lo: Poly aspartic acid peptide-linked PLGA based nanoscale particles: Potential for bone-targeting drug delivery applications. *International Journal of Pharmaceutics* 475(1) (2014) 547-557.
- [14] S.G. Rotman, D.W. Grijpma, R.G. Richards, T.F. Moriarty, D. Eglin, O. Guillaume: Drug delivery systems functionalized with bone mineral seeking agents for bone targeted therapeutics. *Journal of Controlled Release* 269 (2018) 88-99.
- [15] K. Nazemi, P. Azadpour, F. Moztafzadeh, A.M. Urbanska, M. Mozafari: Tissue-engineered chitosan/bioactive glass bone scaffolds integrated with PLGA nanoparticles: A therapeutic design for on-demand drug delivery. *Materials Letters* 138 (2015) 16-20.
- [16] H. Gul, M. Khan, A.S. Khan: 3 - Bioceramics: types and clinical applications. In *Woodhead Publishing Series in Biomaterials, Handbook of Ionic Substituted Hydroxyapatites*, Woodhead Publishing (2020) 53-83.
- [17] R. Mala, A.S. Ruby Celsia: Bioceramics in orthopaedics: A review. In *Woodhead Publishing Series in Biomaterials, Fundamental Biomaterials: Ceramics*, Woodhead Publishing (2018) 195-221.
- [18] K.S. Naik: Chapter 25 - Advanced bioceramics. *Advances in Biological Science Research*, Academic Press (2019) 411-417.
- [19] K. Shanmugam, R. Sahadevan: 1 - Bioceramics - An introductory overview. In *Woodhead Publishing Series in Biomaterials, Fundamental Biomaterials: Ceramics*, Woodhead Publishing (2018) 1-46.
- [20] J. Faig-Martí, F.J. Gil-Mur: Hydroxyapatite coatings in prosthetic joints. *Revista Española de Cirugía Ortopédica y Traumatología (English Edition)* 52(2) (2008) 113-120.
- [21] A.C. Tas, S.B. Bhaduri: Rapid coating of Ti6Al4V at room temperature with a calcium phosphate solution similar to 10x simulated body fluid. *Journal of Materials Research* 19(9) (2004) 2742-2749.
- [22] D.O. Costa, B.A. Allo, R. Klassen, J.L. Hutter, S.J. Dixon, A.S. Rizkalla: Control of surface topography in biomimetic calcium phosphate coatings. *Langmuir* 28(8) (2012) 3871-3880.